FEATURES OF THE WEATHER MODIFICATION ASSESSMENT PROJECT IN THE SOUTHWEST REGION OF SAUDI ARABIA

Paul A. Kucera[1*], Duncan Axisa[1], Roelof P. Burger[2], Don R. Collins[3], Runjun Li[3], Michael Chapman[1], Rafael Posada[4], Terry W. Krauss[5], and Ayman S. Ghulam[6]

[1]National Center for Atmospheric Research, Boulder, CO, USA
[2]University of the Witwatersrand, Johannesburg, South Africa
[3]Texas A&M University, College Station, TX, USA
[4]University of León, León, Spain
[5]Weather Modification Incorporated, Fargo, ND, USA
[6]Presidency of Meteorology and Environment, Jeddah, Saudi Arabia

ABSTRACT. This paper provides an overview of an ongoing rainfall assessment program that has been conducted in the southwest region of Saudi Arabia in the summers of 2008 and 2009 in conjunction with an intensive airborne measurement program. The goal of the study is to examine summertime convection that is observed over the mountainous region (often referred to as the "escarpment") that is adjacent to the Red Sea. The escarpment provides a focus for orographic precipitation as a result of complex interactions with the sea breeze and upper level thermodynamics.

The main interest in the study is to examine clouds that are observed on top of the escarpment. Seasonal precipitation results show two distinct peaks in this region: March-April and August. Evaluation of radar observations during these two peaks indicates the area has distinct characteristics in terms of the diurnal cycle and cell structure. Climatological evaluation indicates there are several distinct precipitation zones in the southwest region.

We have initially focused our airborne research program on summer clouds observed over the escarpment. This paper presents observations of clouds measured by aircraft during an intensive study carried out in the summer of 2009 in the southwest region of Saudi Arabia. A total of 35 research flights were flown during the intensive field campaign during the period 5 August 2009 to 31 August 2009. These flights were conducted under the direction of a flight scientist that assisted the pilot in flight planning and in performing the necessary profiles to accomplish the measurement objectives. Research aircraft operations focused primarily on conducting measurements in clouds that are targeted for cloud top-seeding. Cloud measurements describing the evolution of droplet coalescence, supercooled liquid water, cloud ice and precipitation hydrometeors are necessary to the understanding of precipitation formation.

From this study, we describe the large annual variability in precipitation in the southwest region of Saudi Arabia. Based on our analysis, we have developed a new conceptual model that summarizes the mechanisms for summer precipitation formation in the southwest region. Observations indicate that convective cells tend to be short-lived with complicated microphysics; the presence and concentration of large cloud droplets suggest that GCCN broaden the cloud droplet spectrum; and ice-phase microphysics is important and seems to be efficient. These results have important ramifications for cloud seeding operations.

1. INTRODUCTION

Water stresses often occur in Saudi Arabia. For example, in the absence of permanent surface water, agriculture is largely dependent on irrigation from pumped groundwater, as well as desalination. As stated in a recent United Nations Environment Programme (UNEP) report (http://www.unep.org/geo/geo4/report/06_Regional_Perspectives.pdf), the present rate of groundwater withdrawal threatens near-term depletion of Saudi Arabia's aquifers. Furthermore, with increasing development as well as the increase in population, groundwater contamination has become an additional concern.

Government officials in the Kingdom of Saudi Arabia began a feasibility study to assess the possibility of augmenting rainfall in response to the growing scarcity of freshwater. Scientists from the National Center for Atmospheric Research (NCAR), Texas

*Corresponding author address: Dr. Paul Kucera, National Center of Atmospheric Research/Research Applications Laboratory, PO Box 3000, Boulder, CO 80307; e-mail: pkucera@ucar.edu; phone 1-303-497-2807; fax 1-303-497-8401

A&M University (TAMU), Arizona State University (ASU), University of Witwatersrand (WITS), The University of North Dakota (UND), and Weather Modification, Inc. (WMI) collaborated with scientists from the Presidency of Meteorology and Environment (PME) in Saudi Arabia to carry out the study.

The potential for man-made increases in rainfall using cloud seeding is strongly dependent on the natural microphysics and dynamics of the clouds that are being seeded. The microphysics is dependent on background aerosol levels, because it is the aerosol particles that attract water vapor to form cloud droplets, and in cold clouds, ice particles. In addition, the types and concentrations of aerosol particles can be influenced by trace gases (i.e., air pollution). Given these dependencies, the microphysics of clouds can differ significantly from one geographical region to another, and even between seasons in the same region. In some instances, clouds may not be suitable for seeding, or the frequency of occurrence of suitable clouds may be too low to warrant the investment in a cloud seeding program.

These factors need to be evaluated in a climatological sense or at least over a sufficient period of time to account for natural variations. This requires the conduct of preliminary studies on atmospheric aerosols, cloud microphysics, and dynamics prior to commencing a large cloud seeding effort. If the targeted measurements and additional data show sufficient evidence for clouds to be positively affected by cloud seeding, the cloud seeding technique(s) should then be evaluated using a randomization procedure to statistically demonstrate that the seeding method is effective and measurable. Such a randomized statistical experiment would become the second phase of a future program, which would build on other randomized statistical experiments performed under similar conditions.

Using a combination of radar, aircraft, and surface observations of aerosol, cloud, and precipitation, this project attempts to determine if cloud seeding is a viable option for augmenting freshwater resources in Saudi Arabia. In this project, we are attempting to answer three grand questions:

1. Can seeding clouds in Saudi Arabia increase rainfall at the surface?

2. Under what conditions are seeding techniques viable for increasing rainfall?

3. If rainfall increases are possible, what is the magnitude of the increase attainable over an area, and is the technology cost-effective in serving the water resource needs of Saudi Arabia?

Initially, the assessment program (2006-2007, 2007-2008) was focused on the central region of Saudi Arabia during the winter and spring seasons (November – May). In the summer of 2008, the assessment study shifted to the southwest region of Saudi Arabia. Intensive airborne field programs were conducted in the summer of 2008 and 2009. Because of the vast amount of data collected in Saudi Arabia, only a snapshot of the project can be presented. Therefore, we narrow the focus of the overview to the field programs conducted in the southwest region, with a particular focus on the 2009 observations.

2. PROJECT AREA AND INSTRUMENT OVERVIEW

2.1 Study Region

The Kingdom of Saudi Arabia occupies about 80% of the Arabian Peninsula with an area of approximately 2,250,200 km^2. The Kingdom is bounded by the Red Sea to the west; the Arabian Gulf, UAE, Qatar, and Bahrain to the east; Kuwait, Iraq, and Jordan to the north; Yemen and Oman to the south.

Saudi Arabia comprises several distinct physiographic regions. Eastward from the coastal plain, the Red Sea escarpment rises steeply to the great interior plateaus: the crystalline Najd, the Hismah, and the Hijaz Asir. These highland areas include local mesas, buttes, lava fields, and large and small wadi (e.g., watersheds) systems. Continuing eastward through the sedimentary Najd, to the north of the central region, is the Nafud Basin. The Great Nafud Desert is connected by a long narrow belt of sand (the Dahna) to the largest sand dunes in the world – those of the Ar Rub' Al Khali. Further eastward, in the eastern Province, the downward sloping land surface continues on an even gentler slope to the eastern edge of the Kingdom at the Arabian Gulf.

The project study area is located in the southwestern region in Saudi Arabia (Fig. 1a,b). This region is bounded by the Red Sea to the west, Jeddah to the north, desert highlands to the east, and the Yemen border to the south (see Fig. 1b). As described above, this region is mountainous, composed of mesa, buttes, deep valleys and plateaus. The high elevation is often referred to as the "escarpment". The escarpment rises abruptly from the Red Sea to a maximum elevation of around 2800 m (cyan to white colors on the map, respectively) over horizontal distances of 100 km. This abrupt change in elevation provides the orographic lift for convective storm development, which is the focus of the study.

Figure 1(b) shows a zoomed in view of the southwest region, which was the focal area for the radar study. This region has radar coverage from five radars. The radars are located (from north to south): Jeddah, Taif, Baha, Abha, and Jizan. The radars will be described in more detail in the next section. The final map (Fig. 1c) shows the region of the airborne field study in more detail, which was centered on the Abha radar.

2.2 Radar Network

Five C-band weather radars were utilized during the study. As described above, the radars were located near the cities of Jeddah, Taif, Baha, Abha, and Jizan (e.g., see Fig. 1). Photos of the radar installations are shown in Fig. 2. The radar systems were developed or upgraded by a variety of manufacturers (e.g., Gematronik, Vaisala, and Advanced Radar Corporation [ARC]). They all have Doppler capability. However, the radar located in Baha has the capability to scan in dual-polarimetric mode. For polarimetric scanning, the Baha radar is configured to transmit in a simultaneous horizontal (H) and vertical (V) mode. In this mode, the observed parameters include horizontal radar reflectivity (dBZ_h), differential reflectivity (ZDR), Doppler velocity (VR), spectrum width (SW), differential phase (PhiDP), specific differential phase (KDP), and correlation between H and V polarizations (RhoHV). The readers should refer to Bringi and Chandrasekar (2001) for a detailed description of polarimetric parameters. Analysis of the polarimetric fields is outside the scope of our study. A summary of radar characteristics is provided in Table 1.

The radars continuously scan at a temporal resolution of 5 min and spatial resolution of 0.25 km in range and 1° in azimuth. In volume scan mode, the radars' range in elevation is from 0.5° to 45°. The radars are networked and provide real time information.

For analysis and display of radar observations we used the TITAN (Thunderstorm Identification, Tracking, Analysis, and Nowcasting) software system, which is described by Dixon and Weiner (1993). In addition to TITAN, a new Configurable Interactive Data Display (CIDD) system was also used for

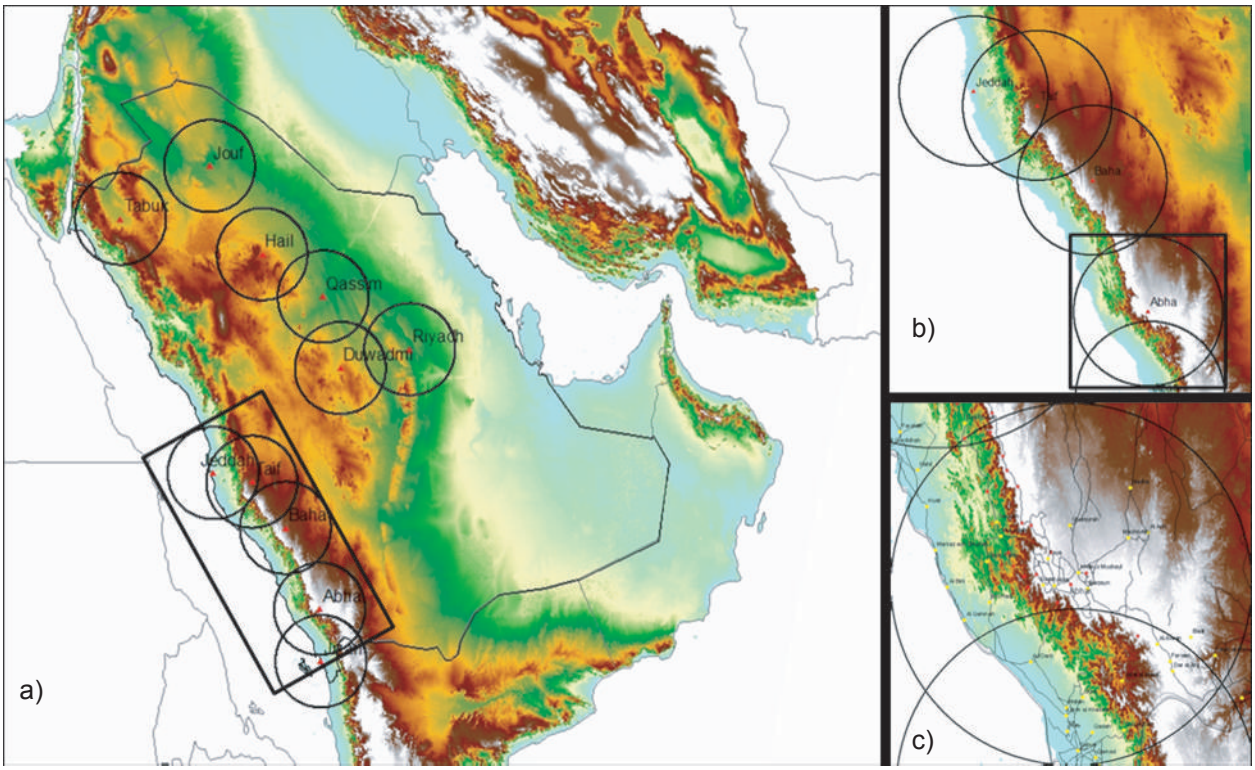

Figure 1: Map showing the project area. Map a) shows the study region (area indicated in the rectangle box) located in the southwest region of Saudi Arabia. Map b) shows the study region in more detail. This region was used in the radar climatology study. Map c) shows the region centered over Abha, which was the focus area for the aircraft sampling studies. In each map, the circles indicate the 150 km range ring for each radar and color background shows terrain features, which ranges from sea level (cyan) to 2800 m (white).

operations and analysis. The TITAN software can display radar data and aircraft position in real-time for the purpose of directing the operations. The CIDD system is routinely set to display an animated 1-hour movie loop of the high resolution polar radar data.

Figure 2: Five radars located in the southwest region of Saudi Arabia: a) Abha, b) Baha, c) Jizan, d) Jeddah, e) Taif. The specifications of the radar are given in Table 1.

Table 1: Radar characteristics for Abha, Baha, Jizan, Jeddah, and Taif.

	Abha	Baha	Jeddah	Jizan	Taif
Description	Gematronik	Vaisala	Gematronik	Gematronik	Gematronik
Frequency	C-Band	C-Band	C-Band	C-Band	C-Band
Type	Doppler	Dual-Pol	Doppler	Doppler	Doppler
Receiver	Vaisala RVP8	ARC HiQ	ARC HiQ	ARC HiQ	Vaisala RVP8
Latitude	18.2287	20.2952	21.7108	16.8963	21.4799
Longitude	42.6607	41.6430	39.1853	42.5835	40.5607

For this study, we used TITAN to determine the diurnal cycle and statistical properties of typical lifetimes, sizes, intensities, and storm movements of the cells. These data will be used to determine if the clouds have the potential to be seeded. This is important in order to understand the number of cells that occur naturally, the length of time that might be necessary in order to perform a later randomized experiment that would quantitatively describe the potential rainfall increase from seeding, to assess the operational aircraft needs in treating these storms in a timely manner, and to estimate the overall area rainfall increases that might be possible from seeding.

2.3 Aerosol Surface Site

Continuous aerosol measurements were made at a surface site located just to the east of the escarpment. The surface and airborne measurements were linked through a repeatedly employed flight pattern that included multiple low-level orbits around the site. Submicron and supermicron size distributions were measured at the surface using a differential mobility analyzer and a TSI, Inc. Aerodynamic Particle Sizer (APS), respectively. A Droplet Measurement Technologies (DMT) CCN counter (CCNc; Roberts and Nenes 2005) was operated together with a tandem differential mobility analyzer (TDMA) to measure supersaturation-resolved CCN concentration and hygroscopic growth of size-resolved particles as the RH to which they are exposed is raised from <15% to 85%.

2.4 Airborne Platform

The WMI Beechcraft King Air B200, hereafter referred to as the WMI King Air, was used as the research aircraft since it was equipped to make cloud microphysical and liquid water content measurements. These measurements are required to address the research objective to study the life cycle of supercooled liquid water content and cloud microphysical properties present in convective towers. The instruments included the Particle Measuring Systems (PMS) Forward Scatter Spectrometer Probe (FSSP-100: Dye and Baumgardner 1984), the DMT Cloud Droplet Probe (CDP), the DMT Cloud Imaging Probe (CIP), the DMT Liquid Water Content (LWC) hot-wire probe and the Stratton Park Engineering Company (SPEC) two dimensional stereo probe (2D-S: Lawson et al. 2006) probe. The cloud physics instrumentation is shown in Figs. 3 and 4. The cloud physics instrumentation payload for the intensive field campaign is listed in Table 2. In addition to the cloud physics instruments, a PMS Passive Cavity Aerosol Spectrometer Probe (PCASP) and a DMA were operated on the aircraft to characterize the below-cloud aerosol size distribution. A pair of DMT CCN counters were operated on board the aircraft in order to provide 1 Hz measurement of CCN concentration at a single supersaturation and slower (~0.002 Hz) measurement of CCN spectra over a range in supersaturation.

The duplication in cloud physics instrumentation proved to be a very important aspect in this project. Since most of the measurements were done in mixed phase convective clouds, shattering of ice crystals at the probe inlets caused by the collision of ice hydrometeors with probe tips forward of the sampling volume (Field *et al*. 2006) complicated the analysis of supercooled cloud droplet and ice crystal size, concentration, and mass that is needed for cloud modification studies and single cloud model

Figure 3: FSSP (left) and 2D-S (right) mounted under the right wing.

Figure 4: PCASP (left) and CIP/CDP/LWC combination probe (right) mounted under the left wing.

Table 2: Cloud physics measurements made by the WMI King Air research aircraft.

Property Measured	Diameter Size Range	Instrument
Cloud droplet particle size	3 to 47 μm, 20 channels	PMS FSSP-100
Cloud droplet particle size	2 to 50 μm, 30 channels	DMT CDP
Cloud hydrometeor size and image	25 to 1550 μm, 62 channels	DMT CIP
Cloud hydrometeor size and image	10 to 1280 μm, 128 channels in horizontal 10 to 1280 μm, 128 channels in vertical	SPEC 2D-S

simulations. Hydrometeor shattering appeared to be most pronounced in the FSSP particle size distribution (PSD) in mixed-phase clouds. The shattering of ice particles on the FSSP sampling inlet and the effect on measurements has raised concerns on the use of FSSP in ice and mixed-phase clouds (Korolev and Isaac 2005). In the presence of irregular large ice crystals FSSP sizing is inaccurate and may detect concentrations an order of magnitude higher than what is believed to be the actual ice particle concentration (Gayet *et al.* 1996). Figure 5 shows the conceptual diagram of the mechanism of particle shattering during sampling by the FSSP. To overcome this issue, measurements with the 2D-S (Lawson *et al.* 2006) were considered alongside the CDP, FSSP and CIP probes. The 2D-S data were processed using criteria-related particle inter-arrival time. Shattering effects on the 2D-S are minimized by removing closely spaced particle images (Baker *et al.* 2009). Shattered fragments have different initial velocities and the distance between them are also different (Korolev and Isaac 2005). The interarrival time between such frames is smaller than the average interarrival time, and it is used as an indicator of shattering events. In the 2D-S, algorithms are used to reject shattered fragments by comparing the particle's inter-particle time to the average inter-particle time for every 10,000 particles. Since the 2D-S has two optical paths (these are labeled as "vertical" and "horizontal" or 2DSV and 2DSH respectively), the particle-by-particle processing algorithms were run independently for the vertical and horizontal path. Figure 6 shows an example of a splashing event and noisy diode data intermixed with 'accepted' data for the vertical optical path. Figure 7 gives an example of particle size distributions (PSDs) calculated using particle-by-particle processing of all particles with no artifact removal (blue trace) and splashing events and noisy photodiodes removed (green trace). In this example the vertical channel has less noisy diodes in the first 5 bins than the horizontal channel. The 2D-S "accepted" data are believed to represent the "actual" particle size distribution and any deviation from the shape of the 2DSV and 2DSH PSD is assumed to be due to shattering artifacts. The orientation of the vertical and horizontal laser beams do not correspond to a horizontal frame of reference. This is due to the probe being installed on a pylon that is perpendicular to the wing dihedral angle. This is also shown in Fig. 3.

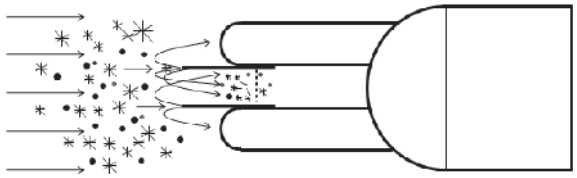

Figure 5: Conceptual diagram adapted from Fig. 16 of Korolev and Isaac (2005) of the mechanism of particle shattering by the FSSP due to the mechanical impact of particles with the FSSP shroud inlet upstream of the sample area. The sample area axis is indicated by the dotted line inside the shroud.

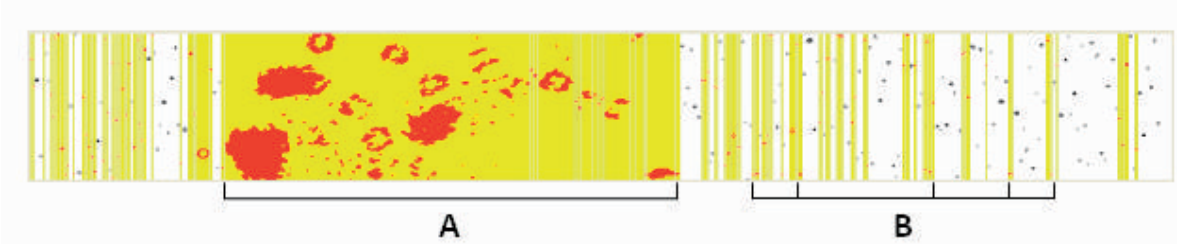

Figure 6: Example of 2D-S splashing event (A) and noisy diode data (B) intermixed with "accepted" particle data for the vertical channel on 11 August 2009 from 11:56:50.151.903.301 to 11:56:50.171.646.603 UTC. The yellow highlighting identifies the "rejected" particles. The height of an image frame is 1280 μm.

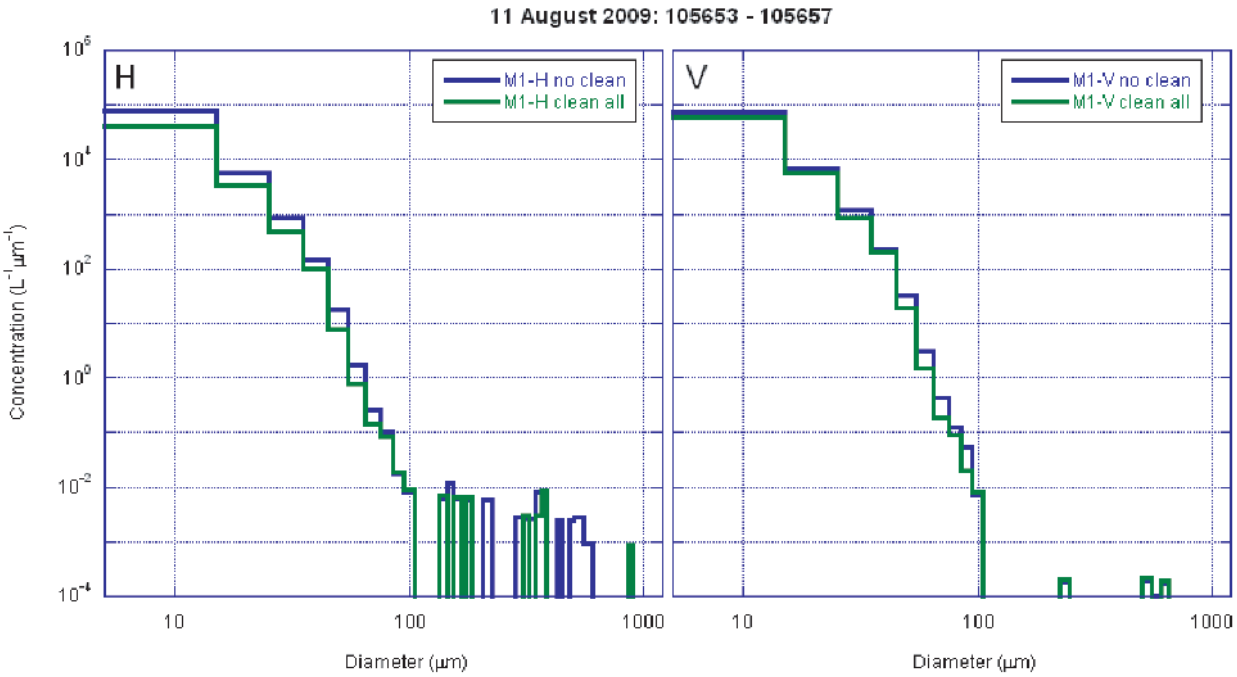

Figure 7: Example of 2D-S mean particle size distribution on 11 August 2009 from 11:56:53 to 11:56:57 UTC. The blue trace ("no clean") includes no artifact removal while the green trace ("clean all") removes splashing events and noisy diode data for the horizontal channel (H) and vertical channel (V).

3. Regional Climatology

The Arabian Peninsula is in many respects a crossroads of the world. Apart from being the cradle of civilization, it also is a crossroads with respect to aerosols in the atmosphere. Large areas of sandy deserts and exposed soil characterize the Arabian Peninsula and surrounding regions, and desert dust lifted aloft in the atmosphere is thus a common feature in the region. Pollution from Europe, especially in the form of sulfates and nitrogen oxides, commonly penetrates the region during the winters and pollution from southwest Asia is very common during the summer. In addition, smoke produced by biomass burning in Africa can also penetrate the region during the summer. Finally, due to the extensive oil industry in the region vast amounts of local pollution are also produced in the form of sulfates that can also affect cloud processes. In addition to the unique dynamic and thermodynamic conditions observed over the Arabian Peninsula, these conditions could either inhibit or enhance natural precipitation processes. This complex interaction between the synoptic scale forcing to the microscale interactions need to be understood and evaluated before a final assessment of cloud seeding to enhance precipitation can be made.

A review of rainfall climatology is an important component in relating the observations from the field campaigns in context of the larger scale, seasonal forcing. Climatologically, Saudi Arabia has a link to the neighboring eastern Mediterranean area. Midlatitude air masses come predominantly from the north and west, and are occasionally deep enough to produce cool weather with scattered rain showers. There is a potential for tropical air masses from the south to influence conditions along the mountains from Yemen and along the Red Sea coast of Saudi Arabia.

Dryness is the prevailing climatic character in Saudi Arabia except in the southwest region. The geographic distribution of rainfall in Saudi Arabia based on a 50-year climatology of rainfall derived from a study by Hijmans *et al.* (2005) is shown in Fig. 8. The precipitation patterns observed in our study are in agreement with the long-term climatology described in Hijmans *et al.* (2005). The southwest region receives annual rainfall > 300 mm due to its unique geographical configuration and interactions of the sea breeze with the escarpment. Rainfall in most of Saudi Arabia is < 200 mm, highly irregular (i.e., large natural variability), and sporadic. In our analysis, we focus on describing the seasonal variability in the southwest region. The goal was to determine when storms occurred and if there were unique sub-regions that have similar precipitation characteristics. This analysis will give valuable insight on when conditions might be viable for

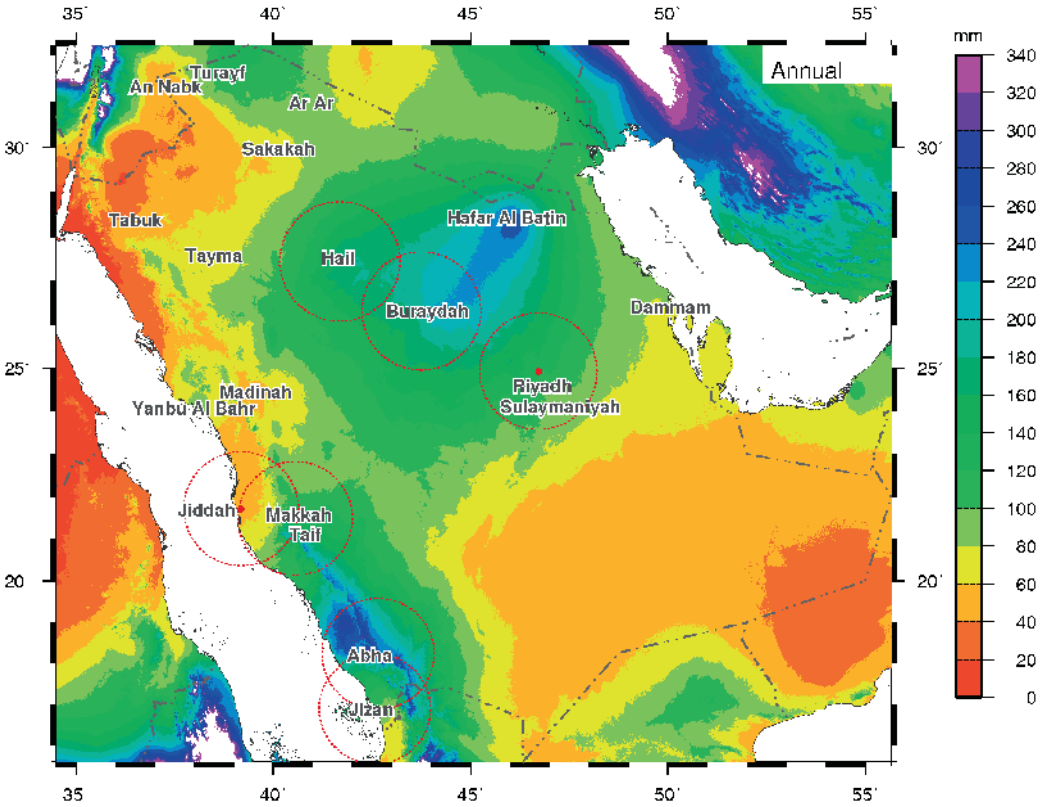

Figure 8: Map of Saudi Arabia showing the distribution of annual rainfall (mm) over Saudi Arabia based on a 50-year surface rainfall climatological record (Hijmans et al. 2005).

seeding and provide regional boundaries that have similar precipitation characteristics. Presumably, in these sub-regions, aerosol, clouds, and forcing mechanisms have similar characteristics for a given season and targeting criteria would be the same.

To determine regions with similar characteristics, we use the precipitation climatology dataset presented in Hijmans *et al.* (2005) and apply a self-organizing map (SOM) technique. The SOM technique uses a neural network algorithm that learns to cluster groups of similar input patterns from high dimensional input fields (e.g., two or three dimensional rainfall fields) in a non-linear fashion into a low dimensional output field (Kalteh *et al.* 2008). The output field is a discrete index that identifies and groups regions that have similar input patterns. The SOM technique has been used successfully to link common circulation patterns in the United States (Hewitson and Crane 2002) and rainfall patterns in Spain (de Luis *et al.* 2000).

Our SOM analysis of the precipitation fields in the southwest region of Saudi Arabia is shown in Fig. 9a. Based on the SOM stratification, there are nine distinct sub-regions or areas that have similar precipitation features that were identified within our study area. The seasonal trend in precipitation for these nine regions is shown in Fig. 9b. It is interesting that the unique precipitation areas have an association with the location of the escarpment (e.g., below to the west, directly on top, to the east). For illustration, the following discussion focuses on the four sub-regions that are observed within the range of the Abha radar. One region is composed of a narrow band that is located on top of the escarpment. Figure 9b indicates this region has two distinct peaks in rainfall. The first peak and maximum peak occur in the months of March and April. A secondary peak is observed in August. Also, the region is associated with some of the largest amounts of rainfall in the southwest regions (and in all of Saudi Arabia). The region that is adjacent to the escarpment located to the east (dark red) covers a much broader area. This area also has a bimodal distribution in the seasonal precipitation analysis. Again, there is a maximum peak in March-April and a secondary peak in August. This region also has observed extreme rainfall events.

The other two regions within the range of the Abha radar is the land adjacent to the Red Sea (purple) and the desert highlands (cyan) to the west. Both have distinct rainfall distributions in comparison to those on top of the escarpment. The region near the Red Sea (below the escarpment) receives most

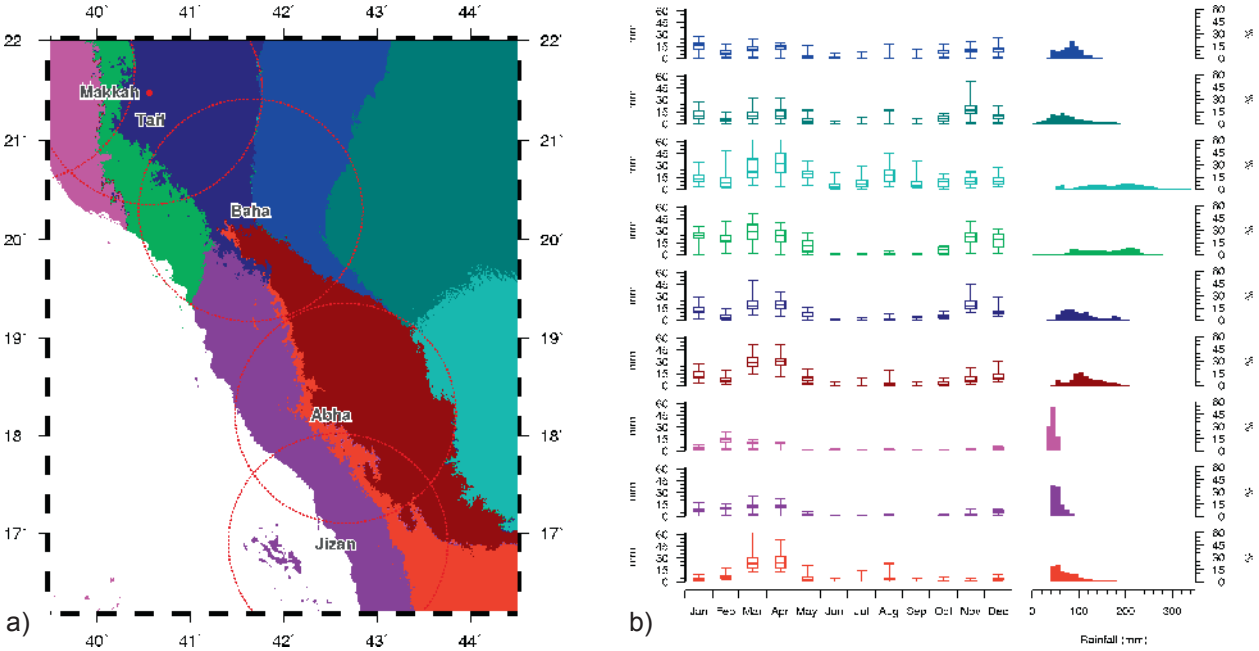

Figure 9: Results of SOM analysis in the southwest region of Saudi Arabia. Panel (a) shows the spatial distribution of the nine regions identified on the SOM analysis. Panel (b) shows the seasonal distribution of rainfall based on the SOM categorization.

of its precipitation during the winter months (November-January). Rainfall tends to be light during the peak in the rainy season. The desert highlands to the east has maximum peak in rainfall in the spring (March-April) without the secondary peak in the summer months. Rainfall accumulations in this region also tend to be less than precipitation observed over the escarpment.

This analysis indicates there are two periods in which we can focus our efforts to study the feasibility of seeding for clouds that are located near or on top of the escarpment (our region of interest). Based on this analysis, we have focused our intensive airborne field program on the summer peak in August. However, we are planning to conduct a study of spring clouds in future field programs.

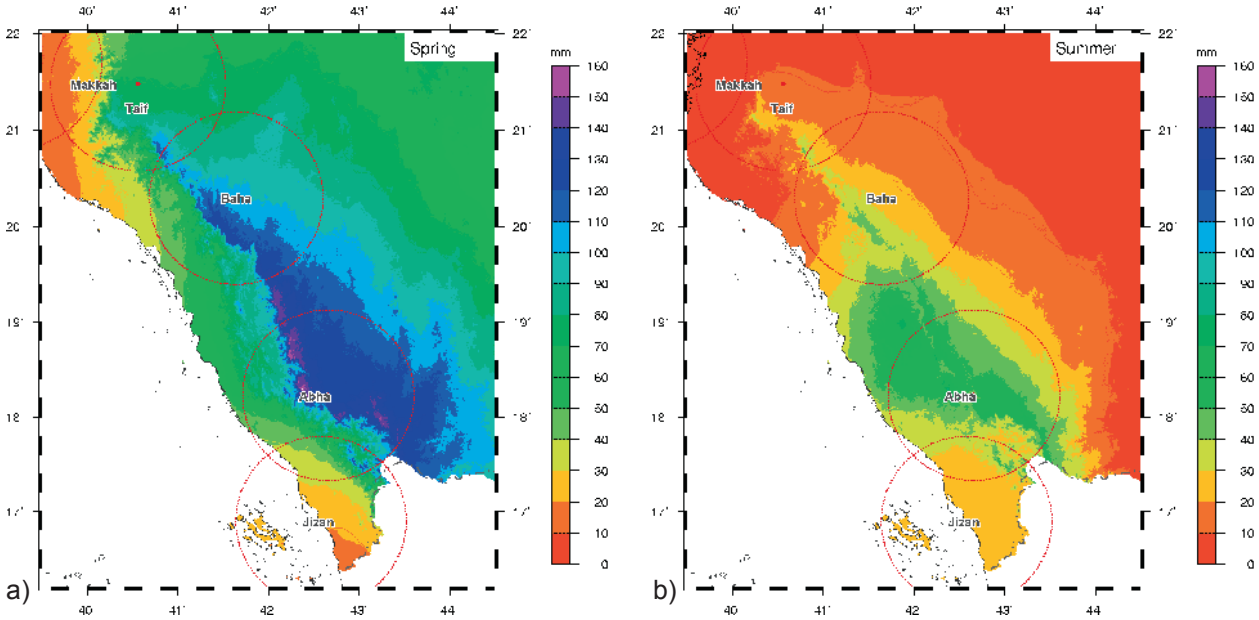

Figure 10: Spatial distribution of rainfall in the southwest region of Saudi Arabia for a) spring (March-May) and summer (June-August).

The spatial distribution of spring rainfall and summer rainfall is shown in Figs. 10a and 10b, respectively. As expected, the rainfall patterns during the spring and summer follow the terrain features along the escarpment. The peak in rainfall is located along the highest peaks to the north and southeast of Abha. Maximum rainfall observed is about 160 mm. The rainfall pattern extends eastward over the escarpment highlands with very little rainfall occurring below the escarpment. The summer rainfall has a different pattern. A peak is also observed on the top of the escarpment. However, it is about a factor of 2 less than the spring peak. It is interesting to note that there is a region of higher rainfall below the escarpment. This area is adjacent to the highest mountain peaks. There can be strong easterly upper level steering winds that propagate the storms westward after developing at the top of the escarpment. Overall, the spring and summer rainfall patterns are consistent with the SOM analysis.

4. OBSERVATIONS FROM THE 2009 FIELD PROGRAM

4.1 Meteorological Summary

During the summer 2009 field campaign, the meteorological conditions varied from the previous field study conducted in the southwest region during 2008. The start of the 2009 season saw a warm dry inversion imbedded in the mid atmosphere, which was not present in four of the previous five years. This inversion acted as a cap to the lower atmosphere and impeded vertical motion and intense convection over this area. Normally, this inversion inhibits convection during the late spring and early summer (May-June). However, these conditions existed for most of the summer 2009. A typical sounding (02 August 2009) for these conditions is shown in Fig. 11.

During the typical summer, the inter-tropical convergence zone (ITCZ) was far enough north by early August to supply moisture to the mid levels of the atmosphere and in turn erode the steep inversion shown in Fig. 11. An example sounding (12 August 2009) for a more unstable atmosphere is shown in Fig. 12. An evaluation of the thermodynamic conditions in the latter part of the month showed a influx of moisture from the ITCZ and the erosion of the inversion during the final week of the field study, which is more typical for atmospheric conditions for this time of year.

An analysis of the radiosonde observations for Abha (OEAB) during the month of August over the previous ten years was performed and the results (Table 3) showed that the strong inversion during August 2009 was not necessarily anomalous although it occurred at a different time than for the 2008 field campaign. During the preceding ten years seven of the ten years had no strong inversion present at the beginning of the period but one did exist at some point during all ten of those years.

Based on analysis of the dynamic and thermodynamic conditions, we have developed a simplified conceptual model for convection in the southwest

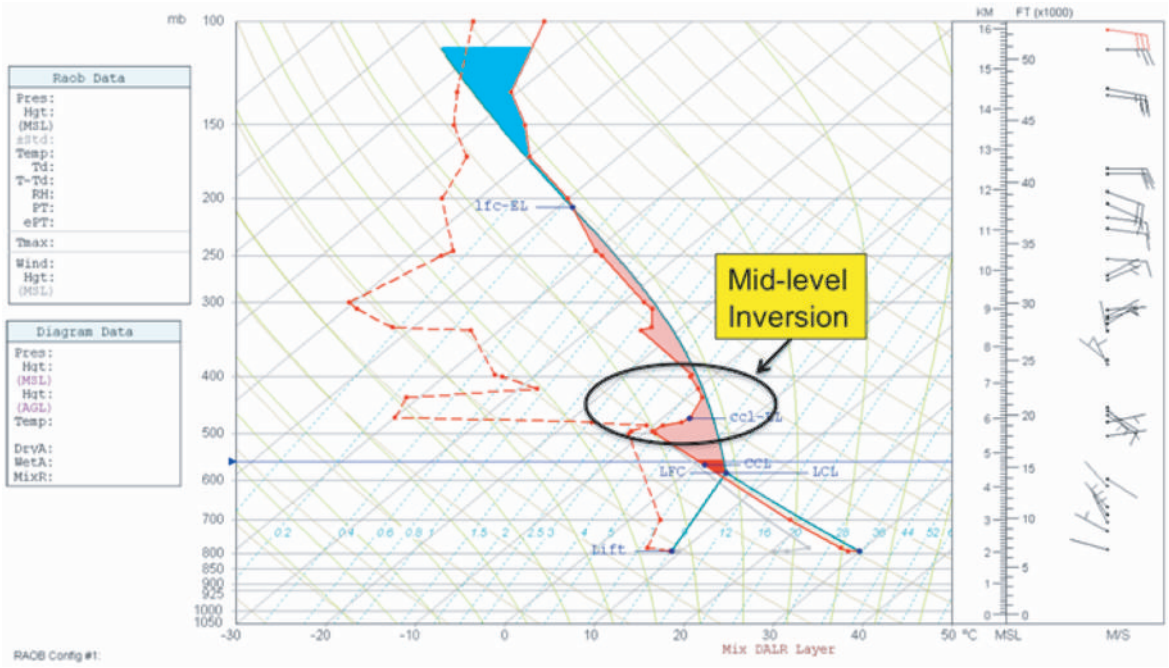

Figure 11: Abha (OEAB) sounding from 02 August 2009 at 0000 UTC.

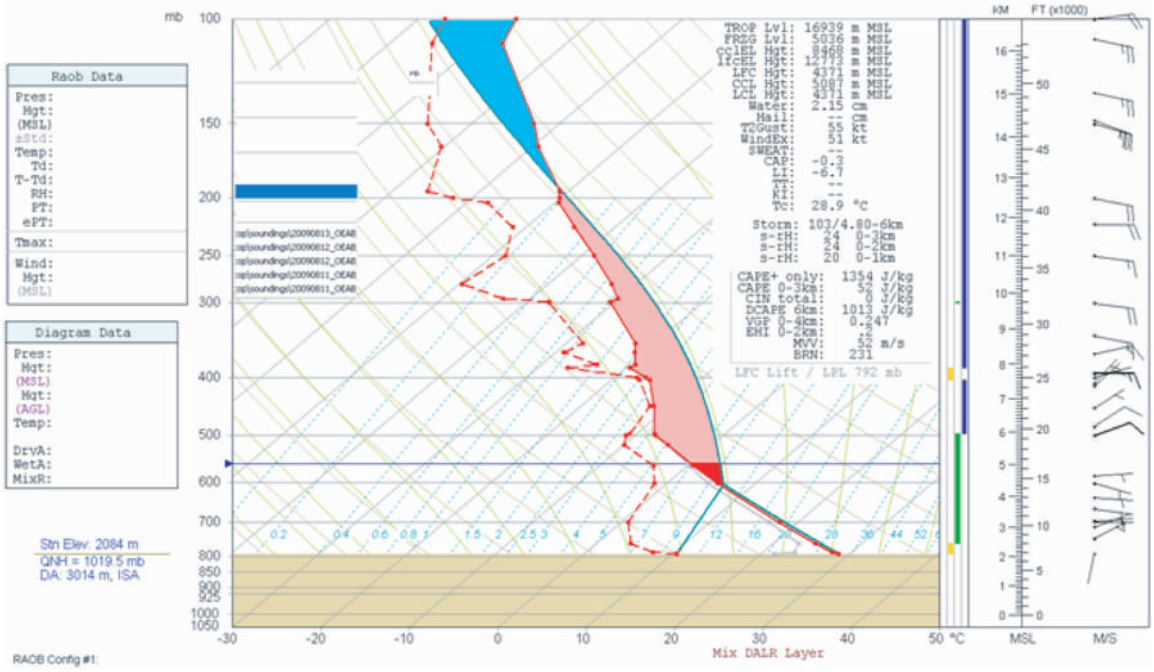

Figure 12: Abha (OEAB) sounding from 12 August 2009 at 0000 UTC.

Table 3: A characterization of each day during August between 1999 – 2009 by the presence of a strong inversion (RED), a weak inversion (YELLOW), no inversion (GREEN), or no data (WHITE) at the mid levels of the atmosphere from the Abha (OEAB) radiosonde database.

	2009	2008	2007	2006	2005	2004	2003	2002	2001	2000	1999
8/1	yes	yes	no	no	yes	no	no	no	no	yes	yes
8/2	yes	yes	no	yes	yes	no	yes	yes	no	yes	yes
8/3	yes	no	no	no	yes	no	yes	NO DATA	NO DATA	NO DATA	no
8/4	yes	no	no	no	yes	no	no	no	no	yes	no
8/5	yes	no	no	no	yes	no	no	yes	yes	no	yes
8/6	yes	no	no	no	yes	no	no	yes	yes	yes	yes
8/7	yes	no	yes	yes	yes	yes	no	NO DATA	yes	no	yes
8/8	yes	no	yes	no	no	no	no	yes	no	yes	yes
8/9	yes	no	yes	no	no	no	no	no	no	yes	yes
8/10	yes	no	yes	no	no	no	no	yes	yes	yes	yes
8/11	yes	no	yes	no	no	no	no	yes	no	yes	yes
8/12	no	yes	NO DATA	no	no	no	no	no	yes	yes	no
8/13	no	yes	NO DATA	yes	no	no	no	no	no	yes	no
8/14	yes	yes	yes	yes	no	yes	no	yes	no	no	no
8/15	yes	yes	yes	yes	yes	yes	yes	yes	NO DATA	yes	yes
8/16	yes	yes	no	NO DATA	yes	yes	yes	yes	yes	yes	no
8/17	yes	yes	yes	yes	yes	yes	yes	yes	yes	no	no
8/18	no	yes	yes	yes	yes	yes	yes	no	yes	yes	yes
8/19	no	yes	yes	yes	yes	yes	yes	no	yes	yes	no
8/20	yes	yes	yes	yes	no	no	yes	no	yes	yes	no
8/21	yes	yes	yes	yes	no	no	no	yes	yes	yes	no
8/22	yes	yes	yes	yes	yes	yes	yes	yes	yes	yes	no
8/23	yes	yes	yes	yes	yes	yes	yes	yes	yes	yes	yes
8/24	yes	yes	yes	yes	yes	yes	yes	yes	yes	yes	yes
8/25	no	yes	yes	yes	yes	yes	no	yes	yes	yes	yes
8/26	no	yes	yes	no	yes	yes	yes	yes	yes	yes	NO DATA
8/27	no	no	no	yes	yes	yes	NO DATA	yes	yes	yes	NO DATA
8/28	no	no	no	no	yes	no	yes	yes	yes	yes	NO DATA
8/29	NO DATA	no	no	yes	yes	yes	yes	yes	yes	NO DATA	NO DATA
8/30	no	no	yes	yes	yes	yes	yes	no	yes	NO DATA	NO DATA
8/31	yes	no	yes	yes	yes	no	yes	no	NO DATA	yes	yes

region of Saudi Arabia, which is shown in Fig. 13. The conceptual model shows that the mid to upper levels are dominated by easterly flow. There is a daily diurnal sea breeze mechanism which creates southwesterly flow from the Red Sea that when orographically lifted along the escarpment induces convective cloud development. To the east of the escarpment, there is a weak to moderate easterly flow from the desert which forces dry air to the region on a daily basis. The interaction between the moist and buoyant airmass from the Red Sea and the dry (and relatively clean) airmass from the desert creates a moisture convergence boundary that becomes the focus for the initiation of convection. The difference in moisture between the two air masses is large with differences in dewpoint temperature of ~20°C. Depending on how strong (or weak) the dry flow from the east is on a particular day, the later (or earlier) convective initiation will occur. On rare days when the easterly flow at the surface is particularly strong and the mid-level inversion is present, convective initiation over the southwest region may not occur at all.

4.2 Radar Observations

In support of cloud seeding feasibility study in the southwest region of Saudi Arabia, we have been archiving data from the network of five C-Band radars (Abha, Baha, Jeddah, Jizan, and Taif) located in this region. Data have been quality controlled to remove ground clutter and spurious echo. Data from each radar have been merged into a common grid using TITAN. The TITAN storm track algorithm has been applied to the merged dataset. The algorithm was used to identify cells associated with precipitation features. For this analysis, a TITAN cell was defined as a continuous reflectivity area equal or greater than 30 dBZ. Many attributes of each cell is then computed by the TITAN algorithm. This section highlights some of the key characteristics of the cells, which include the spatial distribution of cells, the distribution of maximum reflectivity, distribution of cell height, and the diurnal cycle of cell frequency and precipitation flux. The analysis was done on cells observed in summer 2008, summer 2009, and spring 2009 to explore the seasonal differences in precipitation.

The spatial distribution of cells for both spring and summer is interesting to study. The pattern of cell location matches the climatological distribution of rainfall quite well. The cell patterns for spring and summer is shown in Fig. 14a and Fig. 14b, respectively. The observed cells are clearly associated with the location of the escarpment. In the spring, the cells are associated with the mountain peaks south of Abha, west of Abha, and south of Abha toward the Yemen border. The maximum number of cells is observed over Souda Mountain, west of Abha. The maximum number of cells observed in the spring is around 400. It is interesting to observe that no cells are observed west of the escarpment, but there is a broad region of cells observed over the highlands to the east toward the desert region. This analysis supports the long term climatology

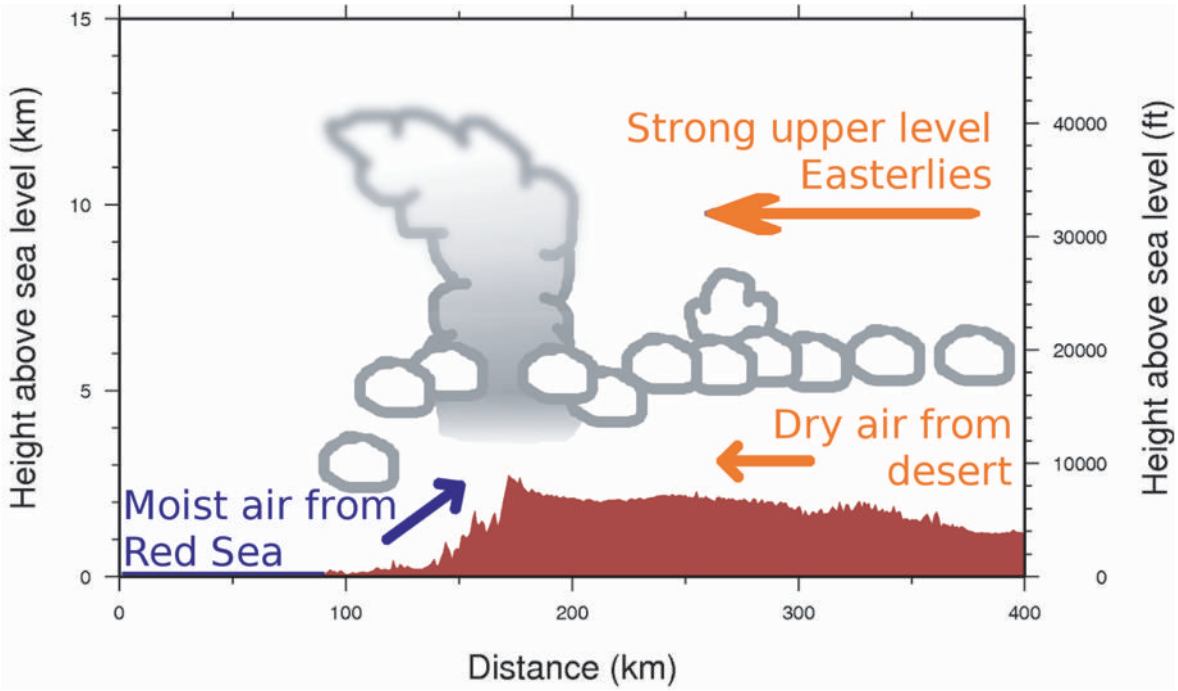

Figure 13: Conceptual model for conditions leading to convective development over the southwest region of Saudi Arabia during the summer.

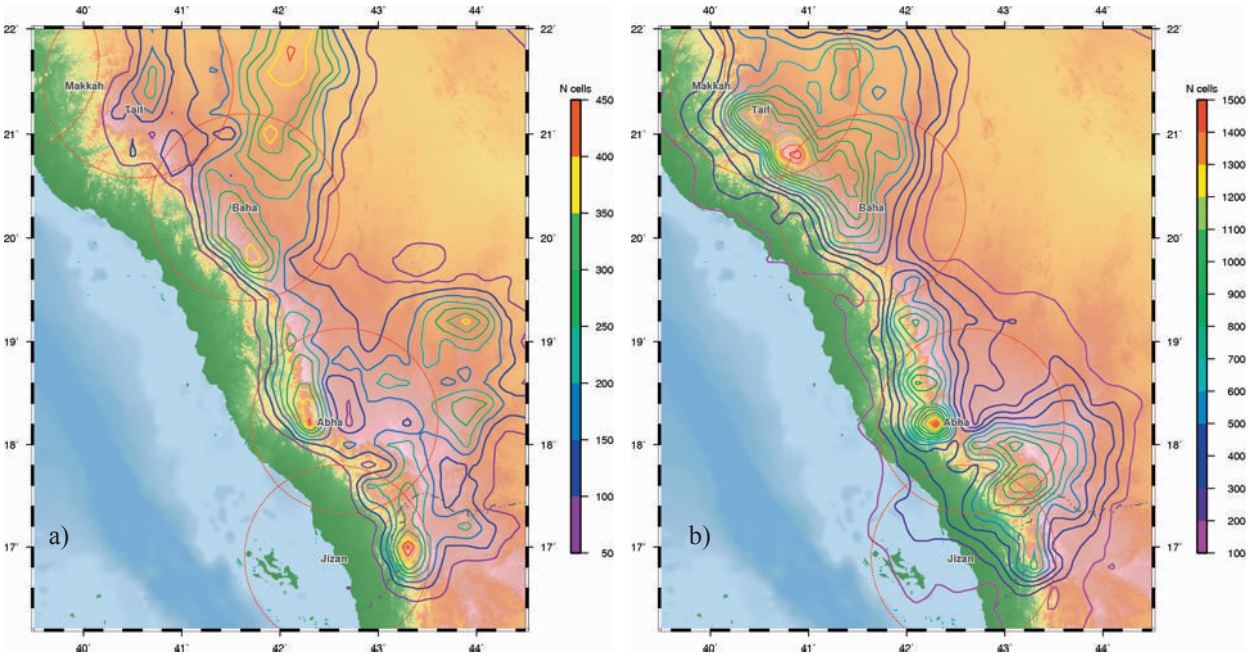

Figure 14: Spatial distribution of number of cells estimate by radar in the southwest region of Saudi Arabia for (a) spring 2009 and (b) summer 2009.

that this region receives a significant portion of the annual precipitation in the spring.

During summer, the peak over Souda Mountain reaches a maximum of over 1500 cells. A secondary maximum was once again located to the southeast of Abha near the Yemen boarder. The number of cells rapidly decreases moving away from the top of the escarpment. However, there is a non-zero number of cells observed west of the escarpment associated with the easterly steering winds moving the storms westward.

It is interesting to note that during the summer season, there is over three times the number of cells observed over certain locations. However, the rainfall observed during the summer is on the order of a factor of two less than spring. This would indicate that in the summer, much of the precipitation observed by radar (e.g., above the surface) does not reach the surface. For both seasons, it is clear that convection is driven by the orographic lift over the escarpment.

The boxplot showing the distribution of maximum reflectivity for summer 2008 (left), summer 2009 (middle), spring 2009 (right) is presented in Fig. 15a. The distributions range from about 26 dBZ to values greater than 65 dBZ. The maximum reflectivity values > 65 dBZ are likely due to ground clutter contamination. However, on occasion, hail was observed with these cells. For summer 2008, the 25% quartile, median, and 75% quartile are 43, 49, and 56 dBZ, respectively. In comparison, the summer 2009 25% quartile, median, and 75% quartile values are 34, 37, and 43 dBZ, respectively. The values for spring 2009 are even lower at 32, 35, and 39 dBZ. This is indicating a large variability in cell intensity between the three seasons. The cells observed in summer 2008 were significantly more intense than in summer 2009. This difference in intensity is likely associated with the strong capping inversion that was observed most of the period. The results indicate spring cells tend to be weaker than cells observed in the summer.

The boxplot of cell heights is shown in Fig. 15b. The distribution is surprisingly different from the trend in maximum reflectivity. With higher maximum reflectivity, it would seem there would be deeper convection. The opposite is observed. For summer 2008, the 25%, median, and 75% quartiles are 3.0, 4.1, and 7.5 km, respectively. The cell heights observed in summer 2009 have a narrow distribution in comparison with the median value of around 7.2 km and lower and upper quartiles ranging from 6.5 km to 8 km. The median cell heights differ on the order of 3 km, which is significant. This needs to be investigated further, but could also be linked to the strength of the capping inversion. The spring cell heights are distributed in between the summer observations. The median cell height for spring 2009 is around 6.5 km and the lower quartile is 5.2 km and upper quartile is 7.5 km.

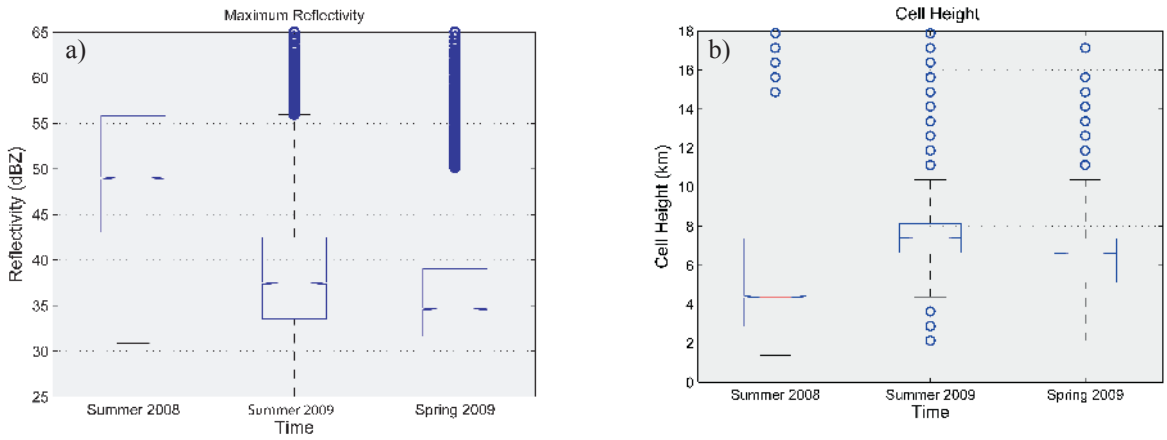

Figure 15: Boxplots showing the distribution of (a) maximum reflectivity and (b) cell height for cells observed in summer 2008, summer 2009, and spring 2009.

The diurnal cycle for cell initiation and cell precipitation flux is shown in Figs. 16a and 16b, respectively. There is a clear signal in the time of cell initiation that is associated with peak in diurnal heating and the timing of the sea breeze interacting with the topography along the escarpment. The summer cells have similar peak in cell occurrence, which occurs around 1400-1600 LT. There are about 200 cells observed each hour during the peak in 2009 compared to 2008. In 2008, the diurnal peak of cells tended to last longer into the evening. Based on the sounding analysis, conditions were more favorable in 2008 for longer periods of storm development. There are a relatively few storms observed during the night time hours. These results would indicate that a daytime seeding operation would be required, which is favorable for safe operations especially since complex terrain is a limiting factor. The spring cells have a distinct distribution. There is a broad late afternoon peak between about 1600 and 2100 LT. For these cells, many would occur after sunset, which could affect seeding operations.

Figure 16b also shows a peak in precipitation flux in the afternoon, which corresponds to the peak in afternoon heating. It is interesting to note that the average precipitation flux in summer 2008 is over a factor of two greater than in 2009. This supports the previous analysis showing the distribution of maximum reflectivity significantly higher in the summer in 2008 than in summer 2009. The precipitation flux analysis indicates that spring storms tend to generate less rainfall on average than summertime storms. These results clearly show there is a significant seasonal variability observed in the storm cells observed in the southwest region. This will make evaluating cloud seeding operations difficult.

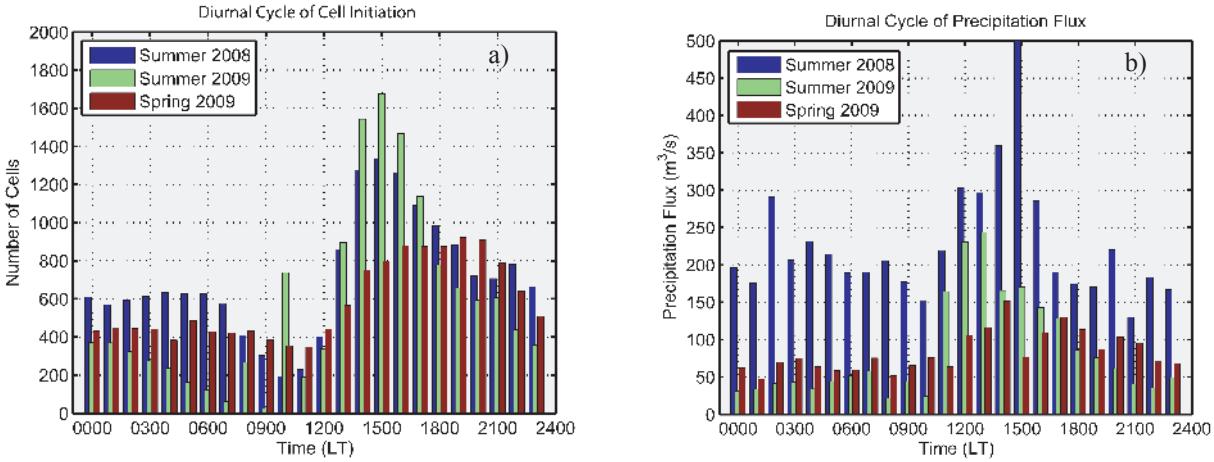

Figure 16: Diurnal cycle of (a) storm cell count and (b) precipitation flux in the southwest region of Saudi Arabia for the summer 2008 (blue), summer 2009 (green), and spring 2009 (red).

4.3 Surface Aerosol Observations

Averaged size distributions and hygroscopic growth distributions measured at the surface site are shown in Fig. 17 and 18. The regional aerosol possessed a persistent accumulation mode that dominated the number concentration even in this arid and dusty region, though supermicron particles accounted for roughly 83% of the particle volume (~mass) concentration. As shown in Fig. 18, the hygroscopic growth distributions of the particles in the accumulation mode size range possess two modes, with the more concentrated of the two comprised of particles having hygroscopicity similar to that of pure sulfate particles. As is evident in the study-average size distributions shown in Fig. 17, the accumulation mode concentration was about twice as high in the air mass behind the sea breeze front as in that ahead of it. Interestingly, the size distribution of the coarse mode and the hygroscopicity and size distribution shape of the accumulation mode differed little in the pre- and post-sea breeze air masses.

4.4 Aircraft Observations

Figure 19 shows the spatial location of flight tracks for the 35 research flights conducted during the 2009 field program. Two main types of flights were conducted during the field program: boundary layer flights and cloud physics flights. The boundary layer flights, shown as a box pattern in Fig. 19, were conducted in the morning hours to document the antecedent aerosol and thermodynamic conditions before convection developed in the afternoon. These flights were also conducted over the surface aerosol site to help determine the link between the surface and the sub-cloud boundary layer.

Cloud physics flights were conducted to document the cumuliform clouds that were observed along the escarpment. Cumuliform clouds were sampled under both warm and supercooled conditions. Deep cumulus clouds were characterized by flying several successively higher constant altitude cloud penetrations. Convective towers that developed on

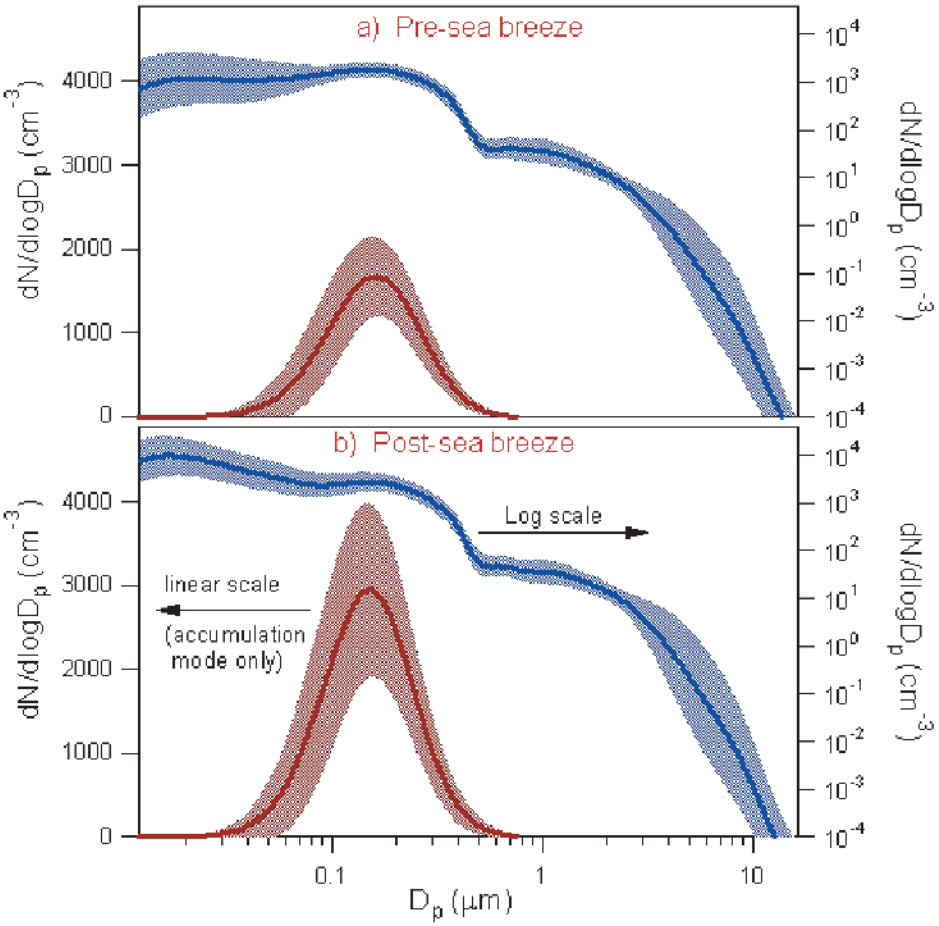

Figure 17: Study averaged aerosol size distributions measured from the surface site. The solid lines represent the mean values and the shaded areas represent ±1 arithmetic (linear scale) or geometric (log scale) standard deviation.

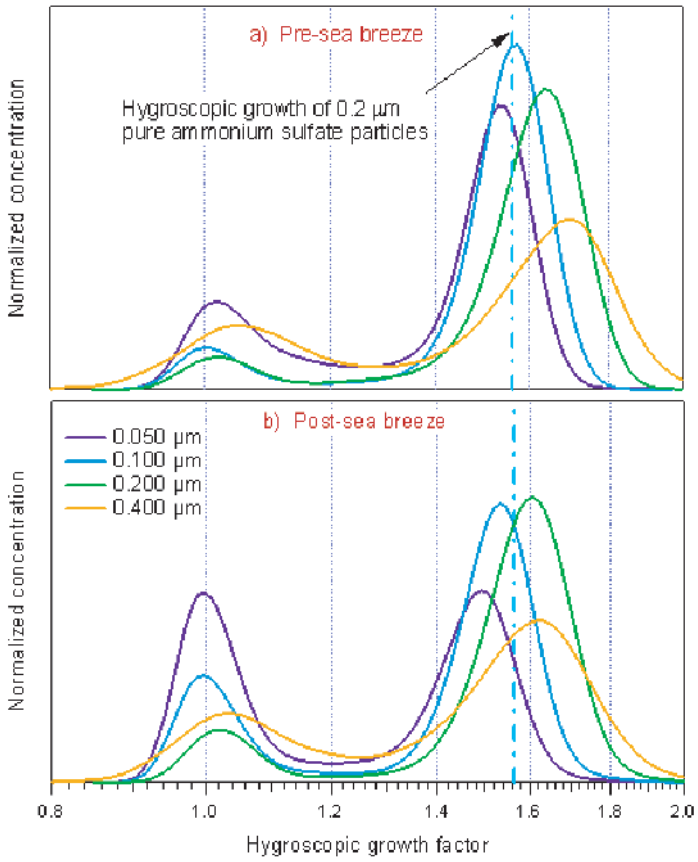

Figure 18: Study averaged aerosol hygroscopic growth distributions measured from the surface site.

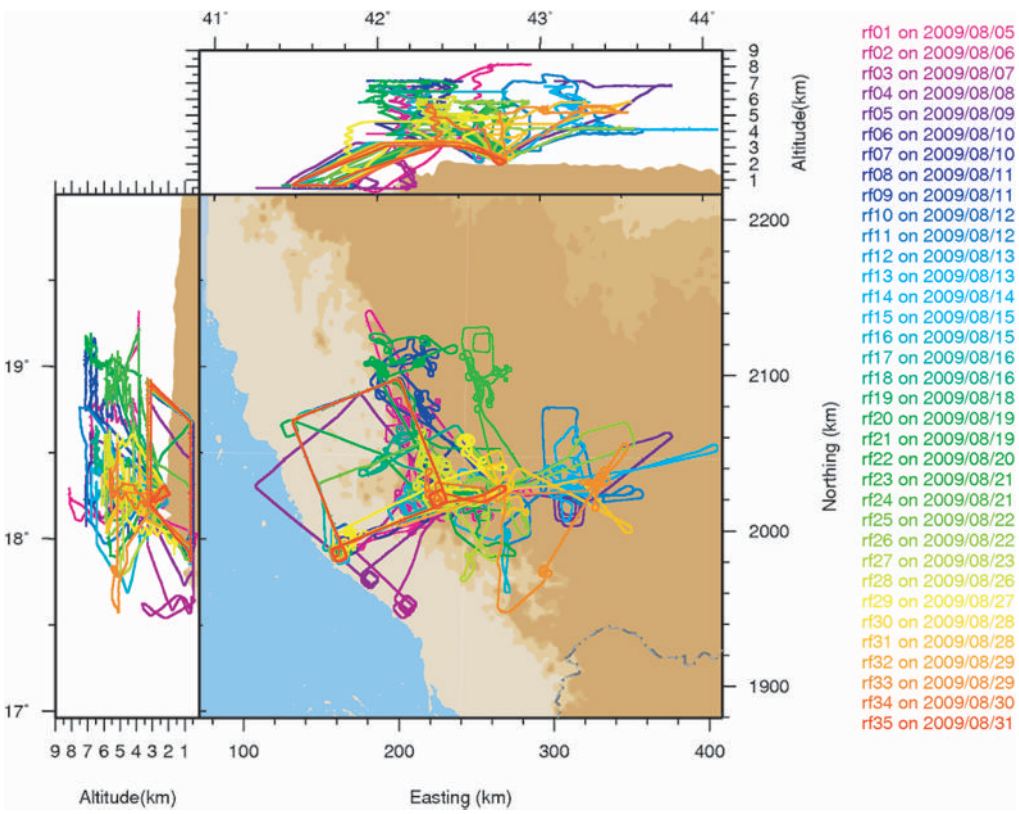

Figure 19: Flight tracks over the southwest region of Saudi Arabia during the 2009 field program.

top of the stable inversion were characterized by flying at the convective cloud top just above the inversion. Aerosol measurements were made above the instrumented surface site and during the climb to cloud base height. The aircraft pilots, who are knowledgeable in the interpretation of heavy precipitation echoes from on-board weather radar, avoid areas of precipitation, associated downdrafts and hail. Therefore most of the cloud penetrations were done in cumulus towers growing above the stable altocumulus inversion, which restricts the dataset to non-precipitating mixed-phase clouds less than 5 km in diameter at 300 m below cloud top. These flights were conducted over the escarpment over an area of complex terrain coinciding with a moisture gradient and an area of enhanced convection.

In general the FSSP and CDP PSDs were described by a similar size distribution; however, the CDP measured a higher concentration of droplets than the FSSP. At a size of 15 µm, the tail of the size distribution of the FSSP diverges from that of the CDP, with the FSSP measuring higher concentrations, greater than an order of magnitude higher at sizes larger than 20 µm. This divergence is thought to be due to shattering. This divergence is also observed if the FSSP PSD is extrapolated to the 2D-S. The CDP matches well with the 2D-S when the PSD is extrapolated along a straight line, implying that the CDP and 2D-S are reasonable in the overlapping range. The CIP particle number concentration is lower than the 2D-S in the 25 - 100 µm range and the FSSP and CDP in the 25 - 50 µm range. This is consistent with observations of under counting in optical array probes for particle sizes smaller than 200 µm (Korolev *et al.* 1990). Good agreement between $2DS_V$ and $2DS_H$ is observed consistently.

The 2D-S provides an improved measurement capability in a size range that is very important for observations of the evolution of droplet coalescence and cloud ice. The following analysis describes the PSD in clouds that are targeted for cloud top-seeding in the southwest region of Saudi Arabia. As mentioned earlier, these cumulus towers were growing above a stable altocumulus inversion. Figure 20 is a lifecycle schematic diagram of a convective unit that develops above the stable altocumulus inversion. Figure 21 shows the aircraft flight track for a typical measurement profile on 11 August 2009. This flight is representative of the type of measurements conducted during the observation period. Figure 22 shows a photograph of a convective tower that was sampled on this flight.

The following section describes the evolution of cloud ice by the analysis of PSDs on 11 August 2009. Cloud penetrations were conducted by flying a sequence of constant altitude cloud penetrations varying from the top of the altocumulus layer (stage s) to the convective cloud top in the developing (d) and young mature (m) stage. Pictures of the cloud before penetration are shown in Figure 23. A series of PSDs from 11 August are shown in Figure 24 and Figure 25. Figure 26 shows a time series of the LWC, temperature, FSSP concentrations and 2D-S concentrations. Table 4 shows the cloud penetration data.

The first penetration in this series was P1. The aircraft penetrated a small isolated towering cumulus that was developing in an area with scattered

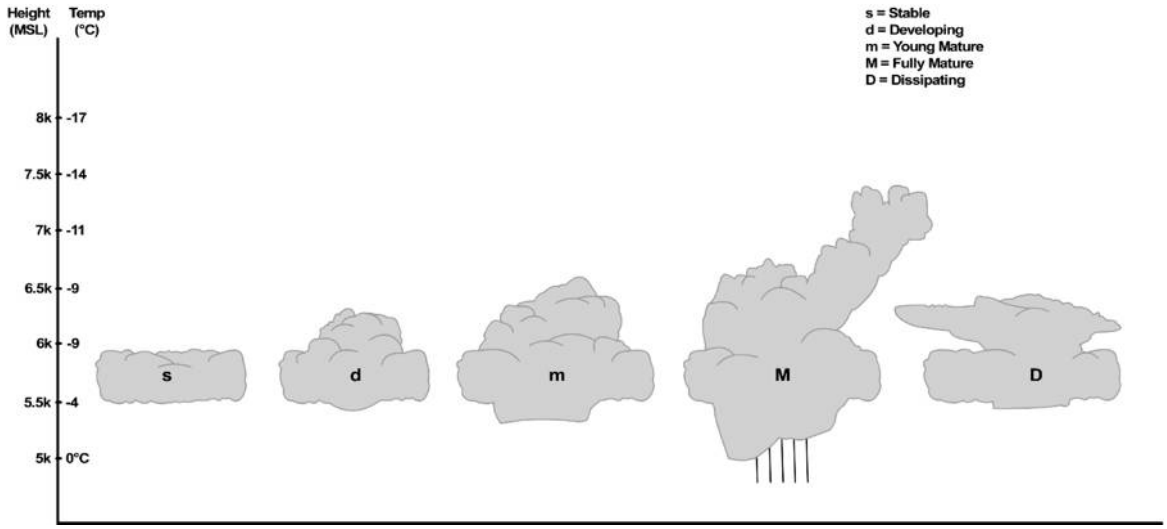

Figure 20: Schematic representation of the southwest region convective lifecycle in a marginally stable atmosphere. The stages represented are: (s) stable; (d) developing; (m) young mature; (M) fully mature; (D) dissipating.

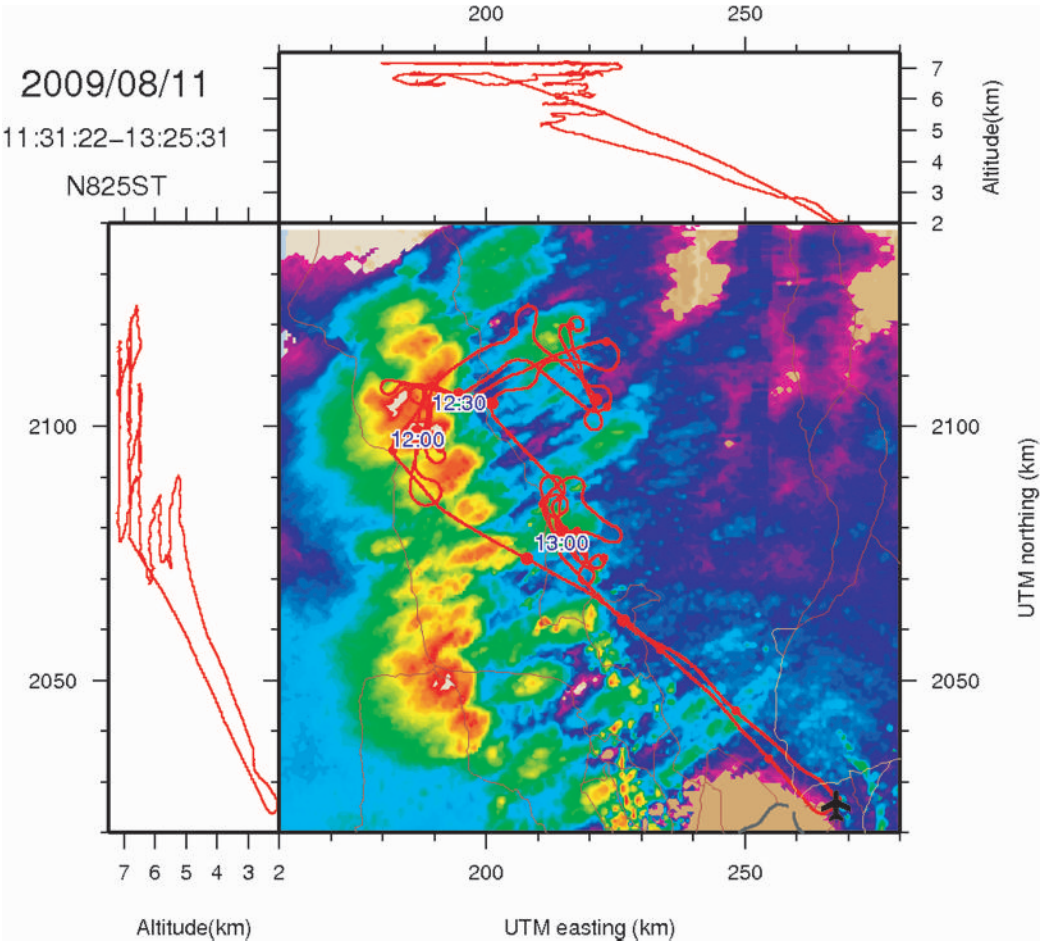

Figure 21: Radar reflectivity overlaid with flight tracks on 11 August 2009.

Figure 22: Photograph taken from the research aircraft on 11 August 2009 of a fully mature (stage M) cloud.

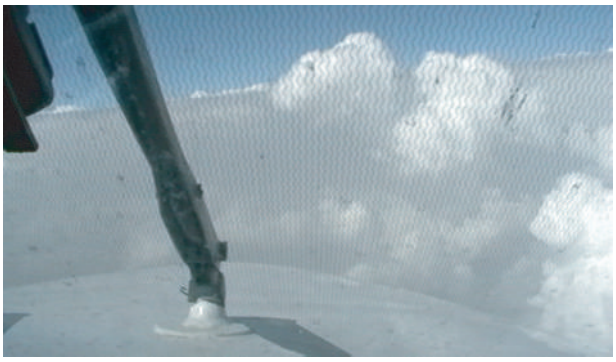

P1 – 11:50:30

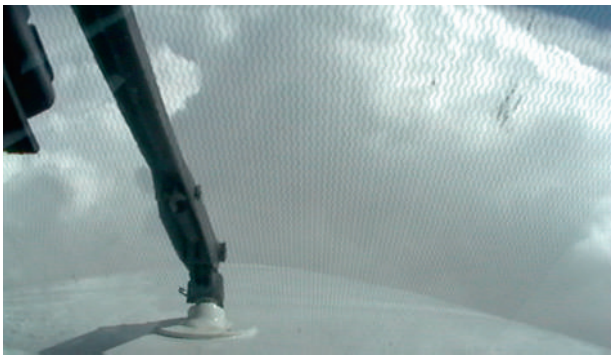

P2 – 11:53:19

P3 – 11:55:59

P4 – 11:58:56

P5 – 12:04:00

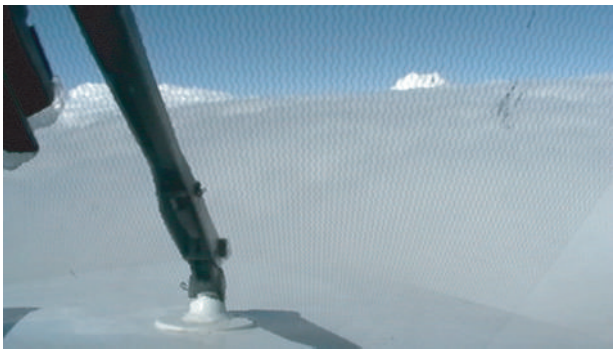

P6 – 12:07:03

Figure 23: Pictures taken from the aircraft video of each cloud before penetration. The text indicates the penetration number and the time the picture was taken. Time is in UTC.

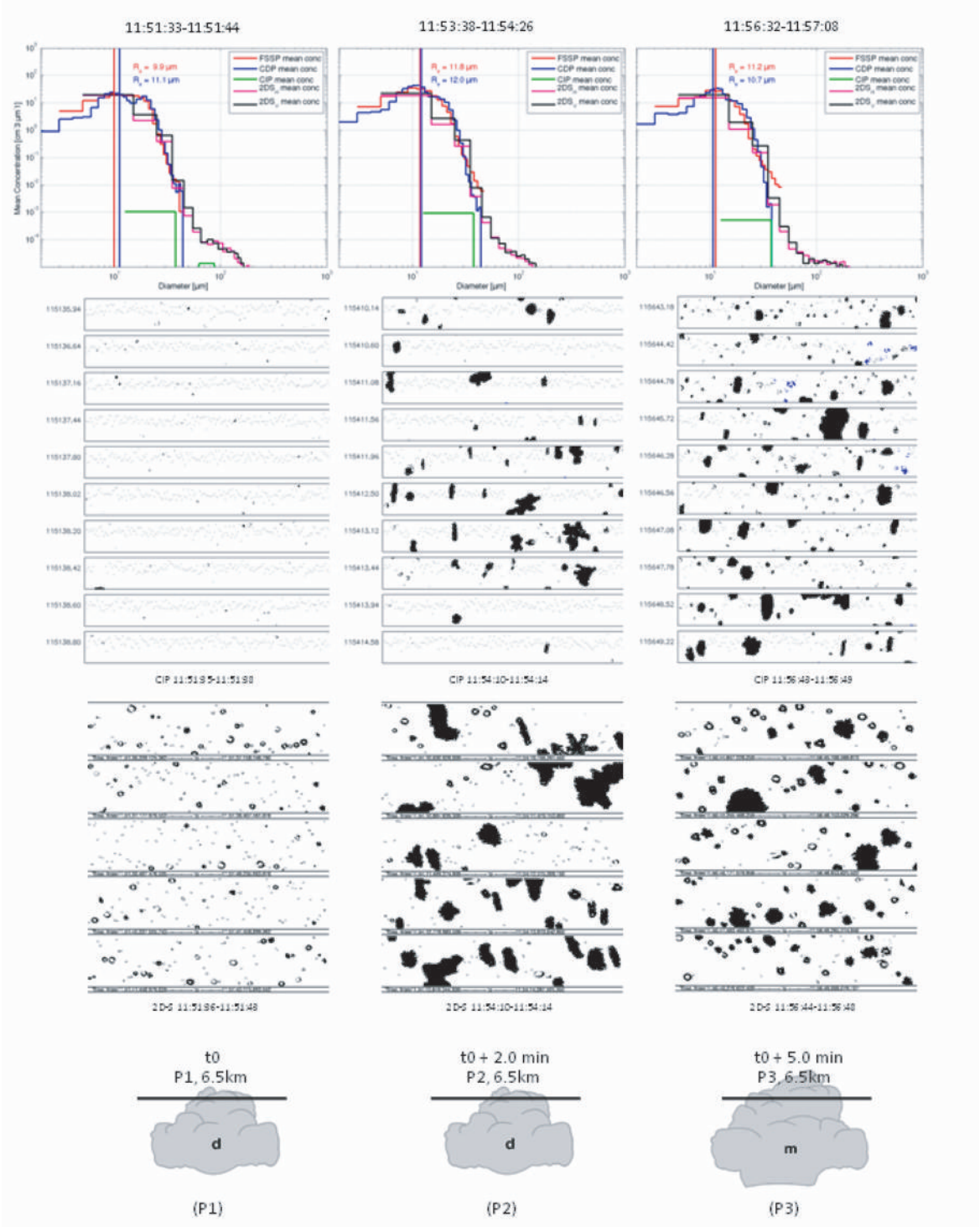

Figure 24: Summary of the microphysical data collected from the aircraft on 11 August 2009 for cloud penetrations P1, P2 and P3. The top figures show the PSDs from the CDP, FSSP, CIP and 2D-S averaged over the period identified in the top of the figure. The middle figures shows a subset of CIP images collected during the cloud penetration. he 2D-S images are shown below the CIP images. The first 50 particles from the $2DS_H$ (excluding end rejects) for the specified time period are shown. The bottom figures show a schematic of the cloud penetration. The height of a CIP image strip is 1550 µm. The height of a 2D-S image strip is 1280 µm.

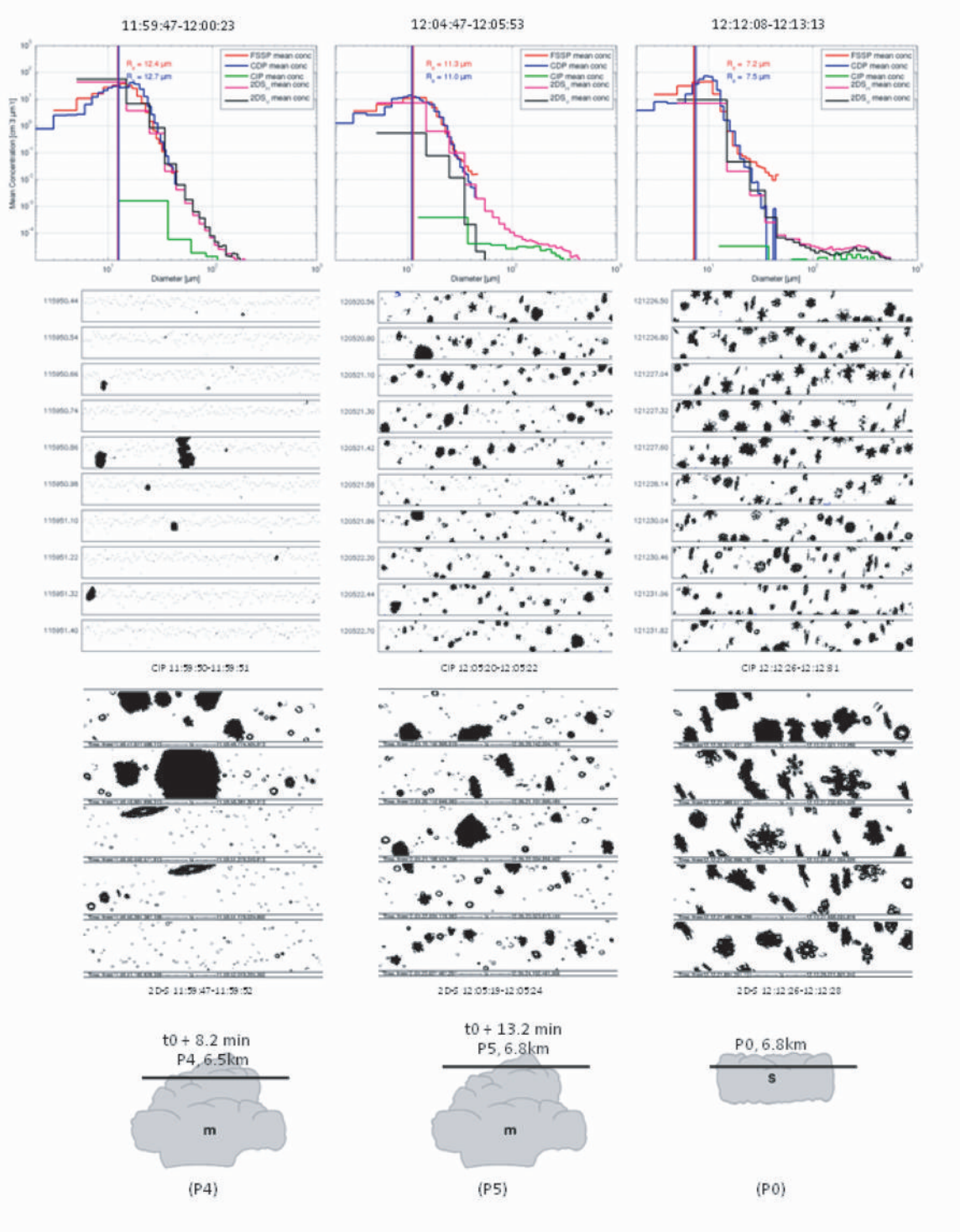

Figure 25: Same as in Figure 20 but for cloud penetrations P4, P5 and P0.

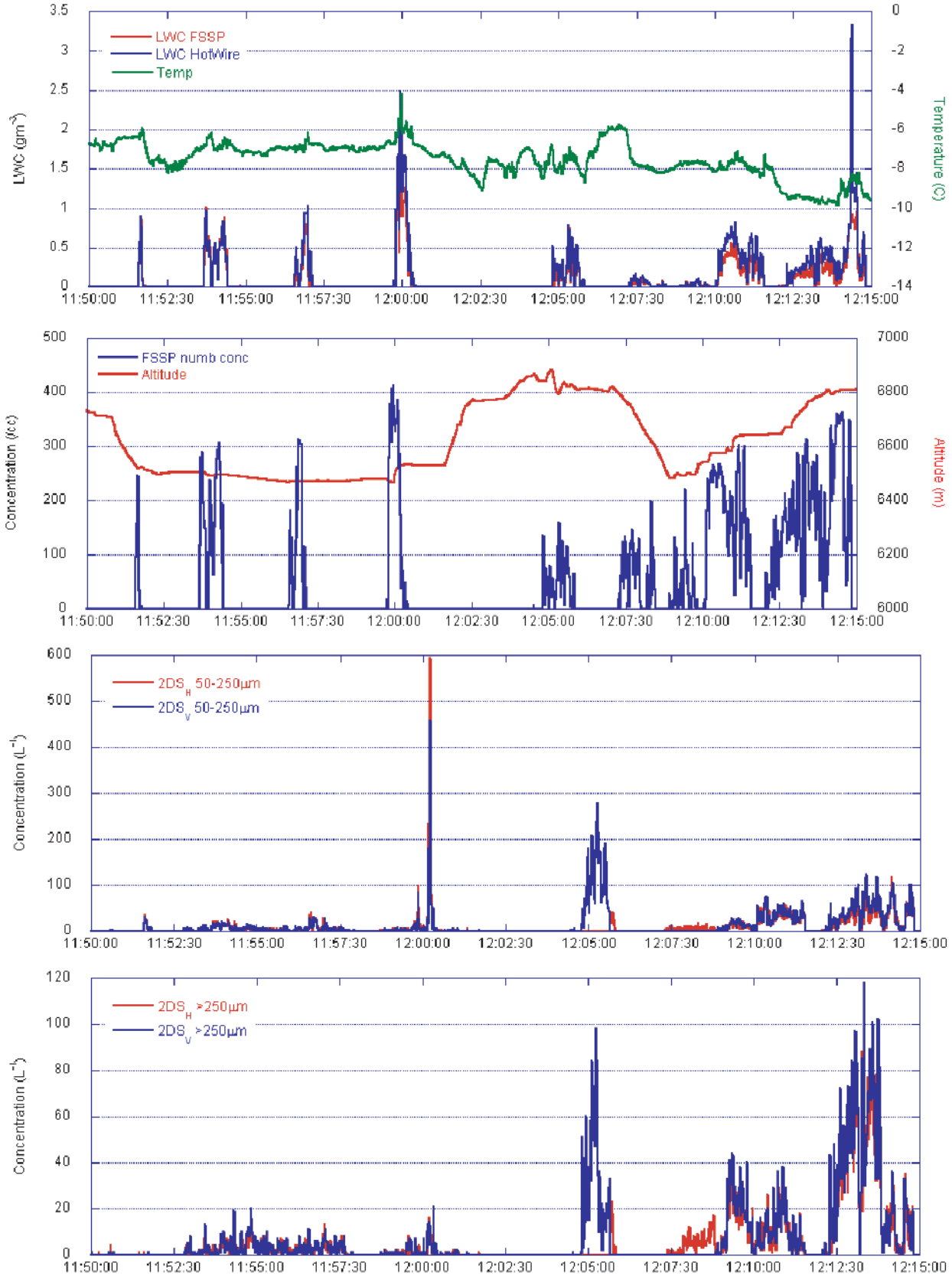

Figure 26: Time series of LWC, temperature, FSSP concentrations and 2D-S concentrations.

Table 4: Cloud physics measurements made by the WMI King Air on 11 August 2009.

Penetration number, stage of development	PSD averaging time	FSSP numb conc (cm^{-3})	LWC (gm^{-3})	Temperature (°C)	Penetration height (km)	Time from first penetration (t_0)
P1, d	11:51:33-11:51:44	470	0.9	-6.0	6.5	t_0
P2, d	11:53:38-11:54:26	520	1.0	-6.5	6.5	t_0 + 2.0 min
P3, m	11:56:32-11:57:08	530	1.0	-7.0	6.5	t_0 + 5.0 min
P4, m	11:59:47-12:00:23	700	2.5	-6.5	6.5	t_0 + 8.2 min
P5, m	12:04:47-12:05:53	500	0.8	-8.0	6.8	t_0 + 13.2 min
P0, s	12:12:08-12:13:13	430	0.4	-9.5	6.8	

altocumulus cover immediately below the cloud formation level. The penetration was done at 6.5 km (-6.0°C) just below cloud top and lasted 11 seconds which indicates that the cloud was about 1.1 km in diameter. The CIP image strips show a large number of the pixel particles, with fewer particles with 3 or 4 pixels. The 2D-S is at 10μm resolution so it adds more detail to the particle shape. The 2D-S images appear to be made up of droplets that vary in number from droplets with a few pixels to larger droplets that are spherical and hollow (out of focus). Detailed inspection of the CIP and 2D-S images suggests that the particles are mostly supercooled liquid water drops (although graupel with smooth edges may be misclassified as water drops in this size range). The PSD plot in Figure 24 shows that the FSSP and CDP effective radius (R_e) are 9.9 and 11.1 μm respectively. Agreement between the CDP and FSSP is good, although the CDP shows a bimodal distribution that is not apparent in the FSSP. This bimodality in the CDP produces a larger R_e. The $2DS_V$ and $2DS_H$ size distributions match the tail of the CDP and FSSP indicating that shattering is not a problem in this case. The excellent agreement between the probes (the CIP is ignored at diameter < 100μm) gives some significance to the bimodality of the CDP. It is important to note that drops as large as 200μm are measured in the tail of the 2D-S size distribution and can also be seen in the 2D-S image strips. Concentrations of particles in the 50-250μm range reach 35/L. These are assumed to be drops.

One can speculate that the bimodality and the broadness of the size distribution may indicate that droplet coalescence is active in the early phases of cloud development. Formation of large droplets in supercooled clouds remains a classical problem in cloud microphysics. The combined growth time of a droplet by condensation and coalescence to a size of, say, 200 μm in a typical cumulus cloud is greater than an hour. This is much greater than the lifetime of small precipitating cumulus clouds. It is not well understood which processes produce fast broadening of the size distribution as is observed here. Some may attribute the source of large droplets to giant cloud condensation nuclei (GCCN) (e.g., Beard and Ochs 1993). In this case 35/L of drops larger than 25 μm is measured. Measurements of the aerosol size distribution indicate that the supermicron aerosol concentration could be as high as 50 cm^{-3} up to heights of 4km in some cases. If a small percentage of this coarse mode aerosol is soluble, then GCCN could be the mechanism by which large droplets form. Others have suggested that stochastic effects during condensational growth of droplets may lead to production of large droplets (Cooper 1989). A uniform supersaturation leads to a narrow size distribution. Turbulent fluctuations in vertical velocities create a fluctuating supersaturation and a broad droplet size distribution. It is also possible that aerosol particles are injected above the altocumulus deck as a result of evaporation leaving a residual hygroscopic aerosol. Evaporated residuals could be larger and/or more hygroscopic than other particles. One possible source of these residual GCCN is the evaporation of coalesced droplets. Explaining how the large droplets form is beyond the scope of this paper; however coalescence due to GCCN, entrainment mixing, variable

supersaturations and cloud processing of aerosol are all viable mechanisms for droplet growth in southwest region clouds.

The subsequent penetration was done 2 minutes later at the same altitude and a temperature of -6.5°C when the cloud was still in the development stage. Figure 23 shows that the cloud had continued to develop and spread over a larger area. It is estimated that the cloud grew to 4.8km in diameter. Excellent agreement is observed between the cloud probes with the CDP and FSSP R_e being almost equal. No large change is observed in the shape of the PSDs in P1 and P2 although differences in hydrometeor type and concentrations are noted. The CIP and 2D-S image strips show that a small concentration of needles, graupel and dendrites formed. The concentrations of these ice particles >250μm are 20/L. A large concentration of small droplets is also present. The presence of ice particles is uncommon at a temperature of -6.5°C and 2 minutes after the previous penetration when no ice was found. Formation of ice crystals by primary ice nucleation may be possible in the heavily dust loaded aerosol although nucleation freezing temperatures of dust particles from the central region of Saudi Arabia were much lower than -6.5°C. Nevertheless a more detailed analysis including calculations and modeling are needed to understand the occurrence of these ice particles.

P3 was done in the young mature stage of development at a temperature of -7.0°C. This is characterized by a lowering of the cloud base and a predominant ice hydrometeor type. The cloud droplet and ice concentrations are similar to the previous penetration except that no large droplets are found in the 2D-S images. The large droplets (>100μm) quickly freeze to graupel and the smaller droplets (<20μm) are depleted by riming processes.

The subsequent penetration (P4) was also done in a young mature cloud and a temperature of -6.5°C, however, a more vigorous updraft of 16 ms^{-1} was encountered. The FSSP measured a maximum concentration of 700cm^{-3} and a liquid water content of 2.5gm^{-3}. Most of the hydrometeors are cloud droplets; however occasional graupel can be seen in the 2D-S images. The concentration of particles in the 50-250μm range reach 595/L and inspection of the 2D-S images cannot rule out the presence of large droplets. Once again it appears that GCCN could be the source of the large droplets. This time the cloud appears to be feeding from the boundary layer aerosol which would bring a larger concentration of aerosol and GCCN, and therefore a higher concentration of droplets.

P5 is the last penetration of the series at a temperature of -8.0°C. The cloud is still in the young mature stage. The FSSP concentration and liquid water content drop to 500 cm^{-3} and 0.8gm^{-3} respectively. Most of the hydrometeors are now graupel of various sizes below 1mm in size. The PSD shows a broad tail extending from the main body of the droplet mode to 600μm. The concentration of particles in the 50-250μm range drops to 280/L while the concentrations of ice particles >250μm increases to 98/L. This is an indication that riming is very active and the liquid water content is quickly depleted resulting in the growth of graupel.

In order to study the extent of mixing between the convective clouds and the adjacent layered cloud, the aircraft measured the altocumulus layer at 6.8km. This is penetration P0 at a temperature of -9.5°C. The CIP and 2D-S show a mixture of ice hydrometeors types including dendrites, graupel and needles. The altocumulus cloud that was penetrated appeared to be detached from other high level cloud so the presence of dendritic crystals is surprising. Dendritic growth occurs in a temperature region of -12°C to -17°C where large aggregates have a tendency to form (Hobbs et al. 1974). This growth is most marked at about -15°C when the arrival of water vapor over the crystal surface is a maximum (Mason 1953). The altocumulus deck must have interacted with a decaying convective tower reaching colder temperatures for the dendrite to be present. The PSD shows a flat distribution at sizes between 100 to 600μm. A droplet mode is still present in the PSD indicating that the layer consists of mixed-phase hydrometeors. Lack of agreement is observed between the FSSP and the CDP at sizes larger than 20μm. This is attributed to ice shattering on the sampling shroud of the FSSP.

This analysis has demonstrated that duplicate cloud physics probes are needed in order to fully understand the fine details of complex mixed-phase clouds like those that develop in the southwest region of Saudi Arabia region. The 2D-S and CDP combination give more detailed and accurate information in mixed-phase clouds and ice clouds as these probes are less prone to shattering effects. The FSSP showed better agreement with the CDP when ice hydrometeors were not present or found in low concentrations. It was also found that CIP concentrations are too low at sizes < 100 μm.

The southwest region's clouds seem to develop graupel quickly by the freezing of droplets in the 50-200μm range. These large droplets could be the result of GCCN that form by the activation of a small percentage of coarse mode aerosols. Once the large droplets form, these quickly freeze and become graupel. The small droplets (<20 μm) remain supercooled and are important in the growth of graupel

by riming. High liquid water content (>2gm^{-3}) can be encountered once the cloud is in the young mature stage and a cloud base generation area has formed. More boundary layer GCCN are entrained through the cloud base in vigorous updrafts forming more large droplets that quickly freeze into graupel. Graupel up to 1mm in diameter quickly forms and is present in concentrations reaching 100/L. This process produces graupel showers that initiate at temperatures around -8.0°C. Once the showers form the cloud becomes fully mature and quickly dissipates into the altocumulus layer. The altocumulus contains mixed-phase hydrometeors including ice particles that are only observed in clouds with colder tops. The altocumulus may also have a role in releasing GCCN above the inversion layer by the evaporation of cloud hydrometeors at the top of the inversion. The extent of this aerosol regeneration at the altocumulus cloud top is unknown.

5. CONCLUDING REMARKS

This paper provides an overview of an ongoing project in the southwest region of Saudi Arabia. The focus of the study was to examine clouds and precipitation observed on top of the escarpment where most of the cloud seeding occurs. The escarpment provides a focus for orographic precipitation as a result of complex interactions with the Red Sea sea breeze and upper level thermodynamics. We utilized a radar network to evaluate the precipitation features, a surface station to examine surface aerosols, and research aircraft to study aerosol and cloud properties. We presented an evaluation of a long-term, 50-yr rainfall climatology, which shows a distinct peak in rainfall occurring in March-April and in August. A SOM analysis was conducted and it was shown there were nine distinct precipitation regions over the southwest Saudi Arabia. We focused our study on the two sub-regions located on the top of the escarpment. The region along the escarpment is associated with the largest amounts of rainfall in the southwest (and all of Saudi Arabia). The region just east of the escarpment also experiences extreme rainfall events. The region below the escarpment and near the Red Sea receives most of its precipitation in winter months while the desert highlands to the east have maximum peak rainfall in the spring. The peak in rainfall occurs along the highest peaks to the north and southeast of Abha, with the summer rainfall being twice that observed in the spring.

There is a distinct diurnal cycle that was observed in the three seasons that were examined: summer 2008, summer 2009, and spring 2009. A clear signal was found in the time of cell initiation associated with maximum diurnal heating and entrainment of moisture by the sea breeze interacting with the topography along the escarpment. During the summer periods, the maximum peak in storm initiation occurred around 1400 and 1600 LT. The peak in storm initiation during spring was much broader between 1600 and 2100 LT. Analysis of cell characteristics indicated there was large seasonal variability. Cells observed in summer 2008 were the most intense followed by summer 2009 and lastly spring of 2009. Because cells tended to form during the day time, at least for summertime convection, potential seeding operations could be conducted during daylight hours. However, because of the large seasonal variability, evaluating cloud seeding operations could be difficult.

The regional aerosol can be characterized by a persistent accumulation mode having hygroscopic properties consistent with a sulfate-rich aged aerosol. The concentration of particles in the accumulation mode, and consequently the CCN concentration, was considerably higher in the air mass behind the sea breeze as in that ahead of it.

Aircraft measurements have shown that clouds develop graupel quickly by the freezing of droplets in the 50-200μm range. Once the large droplets form, these quickly freeze and become graupel.

A large amount of data has been collected that have provided some understanding on the characteristics of clouds and precipitation in the southwest region of Saudi Arabia. Some of the key insights are (1) Observations have helped confirm and describe large annual variability in precipitation in Saudi Arabia; (2) A new conceptual model is described for summer precipitation formation in the southwest region; (3) Convective cells tend to be short-lived with complicated microphysics; (4) The presence and concentration of large cloud droplets suggest that GCCN broaden the cloud droplet spectrum; (5) Ice-phase microphysics is important and seems to be efficient. This has important ramifications for cloud seeding.

The synoptic scale and micro scale complexities of convective clouds that develop in the southwest region of Saudi Arabia present a challenge in producing a final assessment of cloud seeding for precipitation enhancement. The area of interest, surrounded by a prevailing dry climate, present a unique opportunity of studying cloud seeding technologies in a region where freshwater is scarce. A large investment has been made in obtaining measurements in the Central and Southwest regions of Saudi Arabia. Advancements have been made in measurement capabilities and level of understanding of aerosol-cloud interactions and precipitation properties of the region. Future work includes: (1) more detailed measurements of aerosol and cloud microphysics with a special focus on GCCN and

cloud droplet and ice crystal residuals, (2) hygroscopic seeding experiments focusing on identifying the exact seeded cloud volume with sulfur hexafluoride gas tracer, and (3) glaciogenic seeding following a randomization scheme with strict cloud selection criteria.

Acknowledgements. This assessment study was supported by the Presidency of Meteorology and Environment (PME) in Saudi Arabia through a contract with Weather Modification Incorporated of Fargo, North Dakota.

REFERENCES

Baker, B., Q. Mo, R.P. Lawson, D. O'Connor, and A. Korolev, 2009: Drop size distributions and the lack of small drops in RICO rain shafts. *J. Appl. Meteor. Climatol.*, **48**, 616–623.

Beard, K.V. and H.T. Ochs III, 1993: Warm-rain initiation: An overview of microphysical mechanism. *J. Appl. Meteor.*, **32**, 608–625.

Bringi, V.N. and V. Chandraseker, 2001: *Polarimetric Doppler Weather Radar: Principles and Applications.* Cambridge University Press, United Kingdom, 636 pp.

Cooper, W.A., 1989: Effects of variable droplet growth histories on droplet size distributions. Part I: Theory. *J. Atmos. Sci.*, **46**, 1301–1311.

DeLuis, M., J. Raventos, J.C. Gonzalez-Hidalgo, J.R. Sanchez, and J. Cortina, 2000: Spatial analysis of rainfall trends in the region of Valencia (East Spain). *Int. J. Climatol.*, **20**, 1451-1469.

Dixon, M. and G. Wiener, 1993: TITAN: Thunderstorm Identification, Tracking, Analysis, and Nowcasting—A radar-based Methodology. *J. Atmos. Oceanic Technol.*, **10**, 785-797.

Dye, J.E., and D. Baumgardner, 1984: Evaluation of the forward scattering spectrometer probe. Part I: Electronic and optical studies. *J. Atmos. Oceanic Technol.*, **1**, 329-344.

Field, P.R., A.J. Heymsfield and A. Bansemer, 2006: Shattering and particle interarrival times measured by optical probes in ice clouds. *J. Atmos. Ocean. Tech.*, **23**, 1357–1371.

Gayet, J.F., G. Febvre, and H. Larsen, 1996: The reliability of the PMS FSSP in the presence of small ice crystals. *J. Atmos.Oceanic Technol.,* **13,** 1300–1310.

Hewitson, B.C. and R.G. Crane, 2002: Self-organizing maps: applications to synoptic climatology. *Clim Res*., **22**, 13-26.

Hijmans, R.J., S.E. Camerson, J.L. Parra, P.G. Jones, and A. Jarvis, 2005: Very high resolution interpolated climate surfaces for global land areas. *Int. J. of Climatol.*, **25**, 1965-1978.

Hobbs, P.V., S. Chang, and J.D. Locatelli, 1974: The dimensions and aggregation of ice crystals in natural clouds. *J. Geophys. Res.,* **79** (15), 2199–2206.

Kalteh, A.M., P. Hjorth, and R. Berndtsson, 2008: Review of the self-organizing map (SOM) approach in water resources: Analysis, modeling, and application. *Environ. Modelling and Soft.*, **23**, 835-845.

Korolev, A. and G.A. Isaac, 2005: Shattering during sampling by OAPs and HVPS. Part I: Snow particles, *J. Atmos. Oceanic Technol.* **22** (5), 528–542.

Korolev, A. V., S. V. Kuznetsov, Y. E. Makarov, and V. S. Novikov, 1990: Evaluation of measurements of particle size and sample area from optical array probes. *J. Atmos. Oceanic Tech*., **8**, 514 - 522.

Lawson, R.P., D. O'Connor, P. Zmarzly, K. Weaver, B.A. Baker, Q. Mo, and H. Jonsson, 2006: The 2D-S (stereo) probe: Design and preliminary tests of a new airborne, high speed, high resolution particle imaging probe. *J. Atmos. Oceanic Technol.*, **23**, 1462–1477.

Mason, B.J., 1953: The growth of ice crystals in a supercooled water cloud, *Quart. J. Roy. Meteorol. Soc.*, **79**, 104-111.

Roberts, G.C. and Nenes, A., 2005: A continuous-flow streamwise thermal-gradient CCN chamber for atmospheric measurements. *Aerosol Sci. Technol.*, **39**, 206–221.